Inorg. Chem. **2008**, *47*, 6645−6658

Novel Iron(III) Complexes of Sterically Hindered 4N Ligands: Regioselectivity in Biomimetic Extradiol Cleavage of Catechols

Ramasamy Mayilmurugan,[†] Helen Stoeckli-Evans,[‡] and Mallayan Palaniandavar*[,†]

School of Chemistry, Bharathidasan University, Tiruchirapalli 620 024, India, and Department of Chemistry, University of Neuchatel, Neuchatel, Switzerland

Received December 13, 2007

The iron(III) complexes of the 4N ligands 1,4-bis(2-pyridylmethyl)−1,4-diazepane (L1), 1,4-bis(6-methyl-2-pyridylmethyl)-1,4-diazepane (L2), and 1,4-bis(2-quinolylmethyl)-1,4-diazepane (L3) have been generated in situ in CH_3CN solution, characterized as $[Fe(L1)Cl_2]^+$ **1**, $[Fe(L2)Cl_2]^+$ **2**, and $[Fe(L3)Cl_2]^+$ **3** by using ESI-MS, absorption and EPR spectral and electrochemical methods and studied as functional models for the extradiol cleaving catechol dioxygenase enzymes. The tetrachlorocatecholate (TCC^{2-}) adducts $[Fe(L1)(TCC)](ClO_4)$ **1a**, $[Fe(L2)(TCC)](ClO_4)$ **2a**, and $[Fe(L3)(TCC)](ClO_4)$ **3a** have been isolated and characterized by elemental analysis, absorption spectral and electrochemical methods. The molecular structure of $[Fe(L1)(TCC)](ClO_4)$ **1a** has been successfully determined by single crystal X-ray diffraction. The complex **1a** possesses a distorted octahedral coordination geometry around iron(III). The two tertiary amine ($Fe-N_{amine}$, 2.245, 2.145 Å) and two pyridyl nitrogen ($Fe-N_{py}$, 2.104, 2.249 Å) atoms of the tetradentate 4N ligand are coordinated to iron(III) in a cis-β configuration, and the two catecholate oxygen atoms of TCC^{2-} occupy the remaining cis positions. The $Fe-O_{cat}$ bond lengths (1.940, 1.967 Å) are slightly asymmetric and differ by 0.027 Å only. On adding catecholate anion to all the $[Fe(L)Cl_2]^+$ complexes the linear tetradentate ligand rearranges itself to provide *cis*-coordination positions for bidentate coordination of the catechol. Upon adding 3,5-di-*tert*-butylcatechol (H_2DBC) pretreated with 1 equiv of Et_3N to **1**−**3**, only one catecholate-to-iron(III) LMCT band (648−800 nm) is observed revealing the formation of $[Fe(L)(HDBC)]^{2+}$ involving bidentate coordination of the monoanion $HDBC^-$. On the other hand, when H_2DBC pretreated with 2 equiv of Et_3N or 1 or 2 equiv of piperidine is added to **1**−**3**, two intense catecholate-to-iron(III) LMCT bands appear suggesting the formation of $[Fe(L)(DBC)]^+$ with bidentate coordination of DBC^{2-}. The appearance of the DBSQ/H_2DBC couple for $[Fe(L)Cl_2]^+$ at positive potentials (−0.079 to 0.165 V) upon treatment with DBC^{2-} reveals that chelated DBC^{2-} in the former is stabilized toward oxidation more than the uncoordinated H_2DBC. It is remarkable that the $[Fe(L)(HDBC)]^{2+}$ complexes elicit fast regioselective extradiol cleavage (34.6−85.5%) in the presence of O_2 unlike the iron(III) complexes of the analogous linear 4N ligands known so far to yield intradiol cleavage products exclusively. Also, the adduct $[Fe(L2)(HDBC)]^{2+}$ shows a higher extradiol to intradiol cleavage product selectivity (*E*/*I*, 181:1) than the other adducts $[Fe(L3)(HDBC)]^{2+}$ (*E*/*I*, 57:1) and $[Fe(L1)(HDBC)]^{2+}$ (*E*/*I*, 9:1). It is proposed that the coordinated pyridyl nitrogen abstracts the proton from chelated $HDBC^-$ in the substrate-bound complex and then gets displaced to facilitate O_2 attack on the iron(III) center to yield the extradiol cleavage product. In contrast, when the cleavage reaction is performed in the presence of a stronger base like piperidine or 2 equiv of Et_3N a faster intradiol cleavage is favored over extradiol cleavage suggesting the importance of bidentate coordination of DBC^{2-} in facilitating intradiol cleavage.

Introduction

Oxygen-activating enzymes with mononuclear nonheme iron active sites perform a variety of important biological functions.[1−5] Many of the aromatic environmental pollutant molecules are degraded[6,7] by the widely distributed mono-

* To whom correspondence should be addressed. E-mail: palanim51@yahoo.com.
[†] Bharathidasan University.
[‡] University of Neuchatel.

(1) Feig, A. L.; Lippard, S. J. *Chem. Rev.* **1994**, *94*, 759–805.
(2) Hegg, E. L.; Que, L., Jr *Eur. J. Biochem.* **1997**, *250*, 625–629.
(3) Lipscomb, J. D.; Orville, A. M. In *Degradation of Environmental Pollutants by Microorganisms and Their Metalloenzymes;* Sigel, H., Sigel, A., Eds.; Marcel Dekker: New York, 1992; Vol. *28*, pp 243−298.
(4) Que, L., Jr.; Ho, R. Y. N. *Chem. Rev.* **1996**, *96*, 2607–2624.

10.1021/ic702410d CCC: $40.75
Published on Web 07/02/2008

Scheme 1. Active Site Structures of Intradiol- (A) and Extradiol Cleaving (B) Catechol Dioxygenase Enzymes

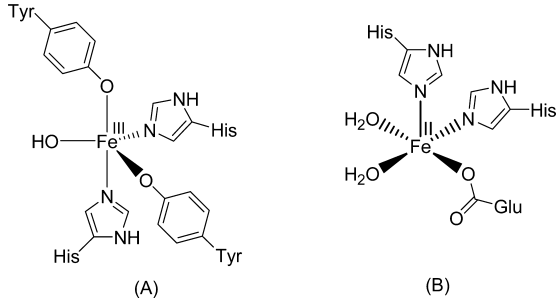

nuclear nonheme family of catechol dioxygenase enzymes, which particularly catalyze the oxidative cleavage[5] of catechols or its derivatives with concomitant insertion of both oxygen atoms of molecular oxygen into the aromatic ring of the substrate resulting in ring cleavage. If two of the hydroxyl substituents in the catechol substrate are in ortho positions then the ring cleavage can occur either between the two hydroxyl groups (intradiol) or between one hydroxyl group and an adjacent carbon atom (extradiol).[8–17] The X-ray crystal structure of the intradiol- cleaving protocatechuate 3,4-dioxygenase (3,4-PCD) enzymes reveals a trigonal bipyramidal iron(III) site with four endogenous protein ligands (Tyr408, Tyr447, His460, and His462) and a solvent derived ligand[10–15] (Scheme 1). Upon substrate (protocatechuic acid, H_2PCA) binding, the active site is altered to a square-pyramidal geometry and the axial Tyr447 and equatorial OH are displaced by the substrate, which binds in a bidentate fashion in its doubly deprotonated form.[16,17] In contrast to intradiol dioxygenases, extradiol dioxygenases contain iron(II) ligated to two histidine, a glutamate ligand, and two water molecules in the active site forming a square pyramidal coordination geometry[17–20] (Scheme 1). The extradiol cleaving enzymes typically require an iron(II) center to utilize an oxygen activation mechanism.[9b,21–23] Interestingly, extradiol cleavage can also be elicited by catechol 1,2-dioxygenases with some substrate analogues,[7,8] which demonstrates that even an iron(III) enzyme can carry out extradiol cleavage chemistry.

A large number of iron(III) complexes have been isolated as models to successfully illustrate the active site structure and function of intradiol-cleaving 1,2-CTD and 3,4-PCD enzymes.[18,19,24–34] Thus, Que and co-workers[26,35,36] synthesized a series of iron(III) complexes of nitrogen, carboxylate

(5) Solomon, E. I.; Brunold, T.; Davis, M. I.; Kemsley, J. N.; Lee, S.-K.; Lehnert, N.; Neese, F.; Skulan, A. J.; Yang, Y.-S.; Zhou, J. *Chem. Rev.* **2000**, *100*, 235–349.

(6) Dagley, S. In *The Bacteria*; Sokatch, J. R., Ornston, L. N., Eds.; Academic Press: Orlando, 1986; Vol. *10*, Chapter 10, pp 527−555.

(7) Levin, M. A.; Gealt, M. A. In *Biotreatment of Industrial and HazardousWaste*; Levin, M. A., Gealt, M. A., Eds.; McGraw-Hill: New York, 1993; pp 5−7.

(8) Que, L., Jr.; Lipscomb, J. D.; Munck, E.; Wood, J. M. *Biochim. Biophys. Acta* **1977**, *485*, 60–74.

(9) (a) Que, L., Jr. In *Iron Carriers and Iron Proteins*; Loehr, T. M., Ed.; VCH: New York, *989*, pp 467−524. (b) Shu, L.; Chiou, Y.-M.; Miller, A. M.; Lipscomb, J. D.; Que, L., Jr. *Biochemistry* **1995**, *34*, 6649–6659.

(10) Ohlendorf, D. H.; Lipscomb, J. D.; Weber, P. C. *Nature* **1988**, *336*, 403–405.

(11) Ohlendorf, D. H.; Orville, A. M.; Lipscomb, J. D. *J. Mol. Biol.* **1994**, *244*, 586–608.

(12) Valley, M. P.; Brown, C. K.; Burk, D. L.; Vetting, M. W.; Ohlendorf, D. H.; Lipscomb, J. D. *Biochemistry* **2005**, *44*, 11024–11039.

(13) Frazee, R. W.; Orville, A. M.; Dolbeare, K. B.; Yu, H.; Ohlendorf, D. H.; Lipscomb, J. D. *Biochemistry* **1998**, *37*, 2131–2144.

(14) (a) Vetting, M. W.; D'Argenio, D. A.; Ornston, L. N.; Ohlendorf, D. H. *Biochemistry* **2000**, *39*, 7943–7955. (b) Elgren, T. E.; Orville, A. M.; Kelly, K. A.; Lipscomb, J. D.; Ohlendorf, D. H.; Que, L., Jr *Biochemistry* **1997**, *36*, 11504–11513.

(15) Vetting, M. W.; Ohlendorf, D. H. *Structure* **2000**, *8*, 429–440.

(16) Whittaker, J. W.; Lipscomb, J. D.; Kent, T. A.; Munck, E.; Orme-Johnson, N. R.; Orme-Johnson, W. H. *J. Biol. Chem.* **1984**, *259*, 4487–4495. (b) Orville, A. M.; Lipscomb, J. D. *J. Biol. Chem.* **1989**, *264*, 8791–8801. (c) True, A. E.; Orville, A. M.; Pearce, L. L.; Lipscomb, J. D.; Que, L., Jr *Biochemistry* **1990**, *29*, 10847–10854.

(17) (a) Orville, A. M.; Lipscomb, J. D.; Ohlendorf, D. H. *Biochemistry* **1997**, *36*, 10052–10066. (b) Orville, A. M.; Elango, N.; Lipscomb, J. D.; Ohlendorf, D. H. *Biochemistry* **1997**, *36*, 10039–10051.

(18) Costas, M.; Mehn, M. P.; Jensen, M. P.; Que, L., Jr *Chem. Rev.* **2004**, *104*, 939–986.

(19) Abu-Omar, M.; Loaiza, A.; Hontzeas, N. *Chem. Rev.* **2005**, *105*, 2227–2252.

(20) Davies, M. I.; Orville, A. M.; Neese, F.; Zaleski, J. M.; Lipscomb, J. D.; Solomon, E. I. *J. Am. Chem. Soc.* **2002**, *124*, 602–614.

(21) Siegbahn, P. E. M.; Haeffner, F. *J. Am. Chem. Soc.* **2004**, *126*, 8919–8932.

(22) Miller, M. A.; Lipscomb, J. D. *J. Biol. Chem.* **1996**, *271*, 5524–5535.

(23) Kovaleva, E. G.; Lipscomb, J. D. *Science* **2007**, *316*, 453–456.

(24) (a) Lauffer, R. B.; Heistand, R. H., II; Que, L., Jr *J. Am. Chem. Soc.* **1981**, *103*, 3947–3949. (b) Heistand, R. H., II; Roe, A. L.; Que, L., Jr *Inorg. Chem.* **1982**, *21*, 676–681. (c) Heistand, R. H., II; Lauffer, R. B.; Fikrig, E.; Que, L., Jr *J. Am. Chem. Soc.* **1982**, *104*, 2789–2796. (d) Lauffer, R. B.; Heistand, R. H., II; Que, L., Jr *Inorg. Chem.* **1983**, *22*, 50–55. (e) White, L. S.; Nilsson, P. V.; Pignolet, L. H.; Que, L., Jr *J. Am. Chem. Soc.* **1984**, *106*, 8312–8313. (f) Pyrz, J. W.; Roe, A. L.; Stern, L. J.; Que, L., Jr *J. Am. Chem. Soc.* **1985**, *107*, 614–620. (g) Que, L., Jr.; Kolanczyk, R. C.; White, L. S. *J. Am. Chem. Soc.* **1987**, *109*, 5373–5380. (h) Funabiki, T.; Sakamoto, H.; Yoshida, S.; Tarama, K. *J. Chem. Soc., Chem. Commun.* **1979**, 754–755. (i) Funabiki, T.; Yamazaki, T.; Fukui, A.; Tanaka, T.; Yoshida, S. *Angew. Chem., Int. Ed.* **1998**, *37*, 513–515. (j) Ogo, S.; Yamahara, R.; Funabiki, T.; Masuda, H.; Watanabe, Y. *Chem. Lett.* **2001**, 1062–1063. (k) Funabiki, T.; Fukui, A.; Hitomi, Y.; Higuchi, M.; Yamamoto, T.; Tanaka, T.; Tani, F.; Naruta, Y. *J. Inorg. Biochem.* **2002**, *91*, 151–158. (l) Funabiki, T.; Sugio, D.; Inui, N.; Maeda, M.; Hitomi, Y. *Chem. Commun.* **2002**, 412–413. (m) Hitomi, Y.; Higuchi, M.; Tanaka, T.; Funabiki, T. *Inorg. Chim. Acta* **2005**, *358*, 3465–3470. (n) Higuchi, M.; Hitomi, Y.; Minami, H.; Tanaka, T.; Funabiki, T. *Inorg. Chem.* **2005**, *44*, 8810–8821. (o) Lim, J. H.; Lee, H. -J.; Lee, K. -B.; Jang, H. G. *Bull. Korean Chem. Soc.* **1997**, *18*, 1166–1171. (p) Bruijnincx, P. C. A.; Lutz, M.; Spek, A. L.; Hagen, W. R.; van Koten, G.; Klein Gebbink, R. J. M. *Inorg. Chem.* **2007**, *46*, 8391–8402. (q) Li, F.; Wang, M.; Li, P.; Zhang, T.; Sun, L. *Inorg. Chem.* **2007**, *46*, 9364–9371.

(25) Yamahara, R.; Ogo, S.; Masuda, H.; Watanabe, Y. *J. Inorg. Biochem.* **2002**, *88*, 284–294.

(26) Jang, H. G.; Cox, D. D.; Que, L., Jr *J. Am. Chem. Soc.* **1991**, *113*, 9200–9204.

(27) (a) Viswanathan, R.; Palaniandavar, M. *J. Chem. Soc., Dalton Trans.* **1995**, 1259–1266. (b) Viswanathan, R.; Palaniandavar, M.; Balasubramanian, T.; Muthiah, P. T. *Inorg. Chem.* **1998**, *37*, 2943–2951. (c) Dhanalakshmi, T.; Bhuvaneshwari, M.; Palaniandavar, M. *J. Inorg. Biochem.* **2006**, *100*, 1527–1534. (d) Palaniandavar, M.; Velusamy, M.; Mayilmurugan, R. *J. Chem. Sci.* **2006**, *118*, 601–610. (e) Palaniandavar, M.; Mayilmurugan, R. *C. R. Chim.* **2007**, *10*, 366–379.

(28) Velusamy, M.; Palaniandavar, M.; Srinivasa Gopalan, R.; Kulkarni, G. U. *Inorg. Chem.* **2003**, *42*, 8283–8293.

(29) Velusamy, M.; Mayilmurugan, R.; Palaniandavar, M. *Inorg. Chem.* **2004**, *43*, 6284–6293.

(30) Velusamy, M.; Mayilmurugan, R.; Palaniandavar, M. *J. Inorg. Biochem.* **2005**, *99*, 1032–1042.

(31) (a) Pascaly, M.; Duda, M.; Rompel, A.; Sift, B. H.; Klaucke an, W. M.; Krebs, B. *Inorg. Chim. Acta* **1999**, *291*, 289–299. (b) Pascaly, M.; Nazikkol, C.; Scweppe, F.; Wiedeman, A.; Zurlinden, K.; Muller.; Krebs, B. *Z. Anorg. Allg. Chem.* **2000**, *626*, 50–55. (c) Duda, M.; Pascaly, M.; Krebs, B. *J. Chem. Soc., Chem. Commun.* **1997**, 835–836. (d) Merkel, M.; Pascaly, M.; Krebs, B.; Astner, J.; Foxon, S. P.; Schindler, S. *Inorg. Chem.* **2005**, *44*, 7582–7589. (e) Merkel, M.; Schindler, D.; Baldeau, S. M.; Krebs, B. *Eur. J. Inorg. Chem.* **2004**, *44*, 783–790.

(32) Merkel, M.; Müller, F. K.; Krebs, B. *Inorg. Chim. Acta* **2002**, *337*, 308–316.

and phenolate donors as structural and functional models for these enzymes and illustrated in detail the intradiol cleavage using substrate activation mechanism. Other research groups have also modeled the intradiol-cleaving enzymes by making use of tetradentate 4N and mono- and bis(phenolate) ligands.[24,25,27–34] We have been also quite successful in isolating iron(III) complexes of tripodal mono- and bis(phenolate) ligands with pyridine/benzimidazole pendants.[27–30] All the above model complexes are found to yield intradiol cleavage products exclusively. However, model complexes capable of eliciting extradiol cleavage are fewer in number[37–41] and have proven far less promising than those for the intradiol-cleaving dioxygenases, though the extradiol cleavage represents the more common pathway for the degradation of aromatic molecules in nature. A few synthetic iron(III)-catecholate complexes based on the tridentate cis-facially coordinating 3N ligands like tiazacyclononane (TACN)[37–40] and hydridotris(3,5-di-*iso*-propyl-1-pyrazolyl)-borate ($Tp^{i\text{-}pr2}$) have been studied as functional models for extradiol cleaving catechol dioxygenase enzymes.[41] Very recently Gebbink et al. have isolated iron(II/III)-catecholate complexes of 3,3-bis(1-alkylimidazol-2-yl)propionate-derived ligands[42] as structural and functional models for these enzymes. We have isolated and studied a number of iron(III) complexes of several linear $3N$[30] and $2NO$[27c] ligands as functional models for the enzymes to correlate the dioxygenation reaction rate as well as extradiol cleavage yields with the ligand steric and electronic factors of the model complexes. Very recently, we have studied a series of iron(III) complexes of linear *N*-alkyl substituted bis(pyrid-2-ylmethyl)amine ligands to find that upon varying the *N*-alkyl groups the extradiol to intradiol cleavage selectivity is systematically tuned.[43]

The successful demonstration that iron(III) complexes of facial tridentate ligands can elicit extradiol cleavage reveals that the presence of a vacant/labile coordination site is essential for extradiol cleavage to occur.[37–43] However, a few iron(III) complexes of tetradentate ligands, which do not have a vacant/labile coordination site in their coordination sphere, also afford extradiol cleavage products.[44] Thus, the iron(III) complexes of tripodal 4N ligands, namely, $[Fe(6\text{-}Me_3TPA)(DBC)]^+$, where 6-$Me_3$-TPA is tris(6-methylpyrid-2-ylmethyl)amine and H_2DBC = 3,5-di-*tert*-butylcatechol, and $[Fe(6\text{-}Me_2BPMCN)(DBC)]^+$, where 6-$Me_2$-BPMCN is *N*,*N*'-dimethyl-*N*,*N*'-bis(6-methylpyrid-2-ylmethyl)-1,2-cyclohexa diamine, elicit measurable amounts (3−20%) of extradiol cleavage products.[44] Also, the iron(III) complex $[Fe(L\text{-}N_4H_2)(DBC)]^+$, where L-$N_4H_2$ is the cyclic tetradentate ligand 2,11-diaza[3,3](2,6)pyridinophane, reacts with O_2 to afford a roughly 1:1 mixture of extradiol and intradiol cleavage products.[45] Further, we have very recently isolated[46] the first tertradentate monophenolate iron(III) complex $[Fe(L)Cl_2]$ [H(L) = *N,N*-dimethyl-*N'*-(2-hydroxy-3,5-dimethylbenzyl)-*N'*-(pyrid-2-ylmethyl)ethylenediamine)], which on treatment with H_2DBC pretreated with Et_3N and on exposure to dioxygen yields regio-selective extradiol cleavage products. This prompted us to study the cleavage of catechols by iron(III) complexes of sterically hindered tetradentate 4N ligands with an aim to tune the regioselectivity to obtain extradiol cleavage exclusively. Here we report a few iron(III) complexes of the tetradentate 1,4-diazepane-based ligands (Scheme 2) as regioselective models for extradiol cleaving enzymes. It is expected that incorporation of 6-methylpyridyl or quinolyl arms in the 4N ligands would regulate the spectral and redox behavior and also tune the dioxygenase activities of these complexes. The X-ray crystal structure of $[Fe(L1)(TCC)]^+$ **1a**, where L1 = 1,4-bis(pyridine-2-ylmethyl)-1,4-diazepane and TCC^{2-} is 3,4,5,6-tetrachlorocatecholate dianion, is a rare example of a monomeric octahedral iron(III) complex with *cis-β* configuration. Remarkably, the present complexes with *cis-β* configuration regiospecifically cleave H_2DBC to yield extradiol cleavage products exclusively. This is remarkable because the iron(III) complex $[Fe(L4)(DBC)]^+$ of the analogous ethylenediamine-based 4N ligand L4 (Scheme 2) with a *cis*-α configuration affords only intradiol cleavage products.[47]

Scheme 2. Structures of Bis(pyridyl/quinolyl) Ligands Used in the Study

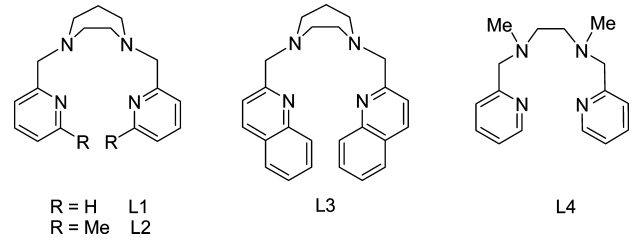

Experimental Section

Materials. Homopiperazine, 3,5-di-*tert*-butylcatechol (H_2DBC), 4-*tert*-butylcatechol (H_2TBC), pyridine-2-carboxaldehyde, 6-methyl-2-pyridinecarboxaldehyde, iron(III) nitrate nonahydrate, iron(III) perchlorate hydrate, sodium triacetoxyborohydride, 2-chloro methylquinoline hydrochloride, *N,N'*-dimethylethylenediamine (Ald-

(33) Pascaly, M.; Duda, M.; Schweppe, F.; Zurlinden, F.; Muller, K.; Krebs, B. *J. Chem. Soc., Dalton Trans.* **2001**, 828–837.
(34) Koch, W. O.; Krüger, H. -J. *Angew. Chem., Int. Ed. Engl.* **1995**, *34*, 2671–2674.
(35) Cox, D. D.; Benkovic, S. J.; Bloom, L. M.; Bradley, F. C.; Nelson, M. J.; Que, L., Jr.; Wallick, D. E. *J. Am. Chem. Soc.* **1988**, *110*, 2026–2032.
(36) Cox, D. D.; Que, L., Jr *J. Am. Chem. Soc.* **1988**, *110*, 8085–8092.
(37) Die, A.; Gatteschi, D.; Pardi, L. *Inorg. Chem.* **1993**, *32*, 1389–1395.
(38) Ito, M.; Que, L., Jr *Angew. Chem., Int. Ed.* **1997**, *36*, 1342–1344.
(39) Jo, D.-H.; Que, L., Jr. *Angew. Chem., Int. Ed.* **2000**, *39*, 4284–4287.
(40) (a) Lin, G.; Reid, G.; Bugg, T. D. H. *Chem. Commun.* **2000**, 1119–1120. (b) Lin, G.; Reid, G.; Bugg, T. D. H. *J. Am. Chem. Soc.* **2001**, *123*, 5030–5039.
(41) Oghihara, T.; Hikichi, S.; Akita, M.; Moro-oka, Y. *Inorg. Chem.* **1998**, *37*, 2614–2615.
(42) Bruijnincx, P. C. A.; Lutz, M.; Spek, A. L.; Hagen, W. R.; Weckhuysen, B. M.; Koten, G.; Klein Gebbink, R. J. M. *J. Am. Chem. Soc.* **2007**, *129*, 2275–2286.
(43) Visvaganesan, K.; Mayilmurugan, R.; Suresh, E.; Palaniandavar, M. *Inorg. Chem.* **2007**, *46*, 10294–10306.
(44) Jo, D.-H.; Chiou, Y. -M.; Que, L., Jr *Inorg. Chem.* **2001**, *40*, 3181–3190.
(45) Raffard, N.; Carina, R.; Simaan, A. J.; Sainton, J.; Riviere, E.; Tchertanov, L.; Bourcier, S.; Bouchoux, G.; Delroisse, M.; Banse, F.; Girerd, J.-J. *Eur. J. Inorg. Chem.* **2001**, 2249–2254.
(46) Mayilmurugan, R.; Suresh, E.; Palaniandavar, M. *Inorg. Chem.* **2007**, *46*, 6038–6049.
(47) Mialane, P.; Tehertanov, L.; Banse, F.; Sainton, J.; Girerd, J. *Inorg. Chem.* **2000**, *39*, 2440–2444.

rich), 3,4,5,6-tetrachlorocatechol (H_2TCC) (Lancaster), protocatechuic acid (3,4-dihydroxybenzoic acid, H_2PCA) (Loba, India), and iron(III) chloride (anhydrous) (Merck, India) were used as received, unless noted otherwise, and H_2DBC was recrystallized from hexane before use. The supporting electrolyte tetrabutylammonium perchlorate (Bu_4ClO_4, G. F. Smith, U.S.A.) was recrystallized twice from aqueous ethanol.

Synthesis of Ligands. 1,4-Bis(2-pyridylmethyl)-1,4-diazepane (L1). To a solution of homopiperazine (0.66 g, 6.62 mmol) and pyridine-2-carboxaldehyde (1.41 g, 13.2 mmol) in CH_2Cl_2 (100 mL) was added sodium triacetoxyborohydride (3.93 g, 18.5 mmol). The mixture obtained was stirred for 12 h, saturated solution of $NaHCO_3$ was added, and the stirring continued for a further 15 min. Then the solution was extracted with ethyl acetate, the organic layer was dried over Na_2SO_4, filtered and reduced to dryness. The oily product was dissolved in THF (50 mL) and treated with NaH (0.17 g, 4.41 mmol) to remove traces of pyridinecarbinol. After stirring the mixture for 90 min, the solvent was removed, and the residue was extracted with several portions of pentane. The pentane extracts were combined, and the pentane removed to give L1 as a brown oil. Yield: 1.03 g (55%). ^{1}H NMR (200 MHz, $CDCl_3$): δ 8.43 (m, 2H), 7.53 (m, 2H), 7.34 (br d, 2H), 7.04 (m, 2H), 3.72 (s, 4H), 2.70 (t, 4 H), 2.65 (s, 4 H), 1.75 (pentet, 2 H).

1,4-Bis(6-methyl-2-pyridylmethyl)-1,4-diazepane (L2). The ligand was synthesized using the procedure employed for L1 but using 6-methyl-2-pyridinecarboxaldehyde instead of pyridine-2-carboxaldehyde.Yield: 0.69 g (56%). ^{1}H NMR (200 MHz, $CDCl_3$): δ 7.45 (m, 2H), 7.23 (br d, 2H), 6.93 (m, 2H), 3.69 (s, 4H), 2.70 (t, 4 H), 2.67 (s, 4 H), 2.44 (s, 6H), 1.74 (pentet, 2 H).

1,4-Bis(2-quinolylmethyl)-1,4-diazepane (L3). 2-Chloromethylquinoline hydro chloride (2.61 g, 12.2 mmol) was taken in ethanol (5 mL) and placed in an ice-bath. To it was added a saturated aqueous solution of K_2CO_3 under vigorous stirring to complete neutralization (pH = 7) and then filtered. Separately, a mixture of homopiperazine (0.61 g, 6.1 mmol) and triethylamine (Et_3N) (1.23 g, 1.7 mL, 12.2 mmol) was prepared in ethylacetate (10 mL). This acid free 2-chloromethylquinoline was added to the solution of deprotonated homopiperazine and stirred for 5 days at 25 °C. After filtration the solvent was removed under reduced pressure to give a dark brown oil from which the desired product was extracted using ethylacetate. The organic layer was dried over anhydrous Na_2SO_4 and the removal solvent afforded the product as viscous brown oil. Yield: 0. 96 g (48%). ^{1}H NMR (200 MHz, $CDCl_3$): δ 8.10 (d, 2H), 8.00 (d, 2H), 7.72 (m, 8H), 4.00 (s, 4H), 3.23 (t, 4 H), 2.87 (s, 4 H), 1.87 (pentet, 2 H).

***N,N'*-Dimethyl-*N,N'*-bis(2-pyridylmethyl)ethylenediamine (L4).** This was synthesized as described previously.[47]

Synthesis of Complexes. ***Caution!*** *During handling of the perchlorate salts of metal complexes with organic ligands care should be taken because of the possibility of explosion.*

In Situ Preparation of Iron(III) Complexes and DBC^{2-} Adducts. The iron(III) complexes (**1**−**4**) of ligands (L1−L4) with general formula $[Fe(L)Cl_2]^+$ were prepared in situ by the reaction of ligands (L1−L4) solution in acetonitrile/DMF solution with a stoichiometric amount of anhydrous iron(III) chloride. The formation of mononuclear iron(III) complexes is evident from the appearance of two bands around 315 and 357 nm and is confirmed byESI-MS,$[Fe(L1)Cl_2]^+$:$(C_{17}H_{22}Cl_2FeN_4)^+$,*m/z*,408;$[Fe(L2)Cl_2]^+\cdot CH_3CN$:$(C_{21}H_{29}Cl_2FeN_5)^+$, *m/z*, 478; $[Fe(L3)Cl_2]^+$: $(C_{25}H_{26}Cl_2FeN_4)^+$, *m/z*, 507.

The adducts [Fe(L)(DBC)] were generated in situ by reacting the complexes **1**−**3** with an equivalent amount of H_2DBC pretreated with 2 equiv of Et_3N and characterized by ESI-MS, $[Fe(L1)(DBC)]^+$: $(C_{31}H_{43}FeN_4O_2)^+$, *m/z*, 558; $[Fe(L2)(DBC)]^+$: $(C_{33}H_{47}FeN_5O_2)^+$, *m/z*, 586; $[Fe(L3)(DBC)]^+$: $(C_{39}H_{47}FeN_4O_2)^+$, *m/z*, 658.

The complexes $[Fe(L1)(TCC)]ClO_4$ **1a**, $[Fe(L2)(TCC)]ClO_4$ **2a**, and $[Fe(L3)(TCC)]NO_3$ **3a** were prepared by using the reported procedure[33] with suitable modifications as follows.

$[Fe(L1)(TCC)]ClO_4$ 1a. To a 2 mL solution (methanol:acetone, 3:2 v/v) of the ligand L1 (29 mg, 0.1 mmol) was added a solution of $Fe(ClO_4)_3\cdot xH_2O$ (35 mg, 0.1 mmol) in the same solvent mixture (2 mL) with stirring. To this was then added a hot solution (2 mL) of tetrachlorocatechol monohydrate (25 mg, 0.1 mmol) dissolved in the same solvent mixture. Piperidine (20 μL, 0.2 mmol) was then added to the reaction mixture, and the reaction mixture refluxed for a few seconds. Dark purple microcrystals of complex **1a** were formed over 12 h upon slow cooling and standing. Yield: 23 mg (41%). Anal. Calcd for $C_{23}H_{22}Cl_5FeN_4O_6$: C, 40.41; H, 3.24; N, 8.20%. Found: C, 40.44; H, 3.22; N, 8.21%. λ_{max}/nm (ε/$M^{-1}cm^{-1}$) (acetonitrile) 303 (7320) and 585 (2010). Single crystals suitable for X-ray crystallography were obtained upon slow cooling and standing of a solution of the complex.

$[Fe(L2)(TCC)]ClO_4$ 2a. This complex was prepared by using the procedure used for isolating **1a** and using ethanol as solvent. A dark purple crystalline complex **2a** was formed over 24 h upon slow cooling and standing. Yield: 26 mg (45%). Anal. Calcd for $C_{25}H_{26}Cl_5FeN_4O_6$: C, 42.20; H, 3.68; N, 7.85%. Found: C, 42.24; H, 3.62; N, 7.87%. λ_{max}/nm (ε/$M^{-1}cm^{-1}$) (acetonitrile) 362 (sh) and 579 (2230).

$[Fe(L3)(TCC)]NO_3$ 3a. This was also prepared using the procedure employed for isolating **1a** and using $Fe(NO_3)_3\cdot 9H_2O$ instead of $Fe(ClO_4)_3\cdot xH_2O$ in ethanol as solvent. Upon cooling and standing for 12 h at room temperature a dark purple powder was obtained. Yield: 38 mg (52%). Anal. Calcd for $C_{31}H_{26}Cl_4FeN_4O_5$: C, 48.50; H, 3.41; N, 7.30%. Found: C, 48.88; H, 3.42; N, 7.26%. λ_{max}/nm (ε/$M^{-1}cm^{-1}$) (acetonitrile) 315 (21470) and 569 (2360).

Kinetics and Reactivity Studies. Kinetic analyses[26–34,43–47] of the catechol cleavage reactions were carried out by time-dependent measurement of the disappearance of the lower energy catecholate-to-iron(III) LMCT band at ambient temperature (25 °C) by exposing the catecholate adducts prepared in situ to molecular oxygen. The solvents were equilibrated at the atmospheric pressure of O_2 at 25 °C and the solubility of O_2 at 25 °C is as follows: acetonitrile, 8.1 $\times$ 10^{-3} M;[34,48] DMF (dimethylformamide), 4.86 $\times$ 10^{-3} M.[28,29,48] A stock solution of the adducts $[Fe(L)(HDBC)]^{2+}$ was prepared by treating the complex **1**−**3** (1.0 $\times$ 10^{-2} M) with an equivalent amount of H_2DBC pretreated with 1 equiv of Et_3N. The adducts $[Fe(L)(DBC)]^+$ were generated in situ by treating **1**−**3** (1.0 $\times$ 10^{-2} M) with an equivalent amount of H_2DBC pretreated with 2 equiv of Et_3N or 1 or 2 equiv of piperidine. Oxygenation was started by rapid delivery of a stock solution (0.1 mL) of the catecholate adducts (1.0 $\times$ 10^{-2} M) by syringe to an O_2-saturated solvent (4.9 mL).

The dioxygenase activities of the present complexes were determined using a known procedure with modifications.[29,43,46] The complexes $[Fe(L)(HDBC)]^{2+}$ or $[Fe(L)(DBC)]^+$ (0.1 mmol) in CH_3CN/DMF solvents (5 mL) were exposed to dioxygen and stirred for 24 h. The oxygenation reaction was quenched by the addition of 6 M HCl (5 mL). The products were extracted from the aqueous solution with CH_2Cl_2 (3 $\times$ 20 mL). For reactions in DMF solvent diethylether was used to extract the oxygenation products. The clear yellow organic layer was separated was dried over anhydrous Na_2SO_4 at room temperature. Further purification of the products

(48) (a) *Japan Chemical Society, Kagaku-Binran Basic Part II*, 2nd ed.; Maruzen: Tokyo, 1975. (b) Sawyer, D. T. *Oxygen Chemistry*; Oxford University Press: New York, 1991.

was accomplished by column chromatography using silica gel and a CH_2Cl_2/CH_3OH (8:1) mixture as eluent. The major products were separated and analyzed by GC, GC-MS, and ^1H NMR techniques. The other minor products were analyzed as a mixture, detected by GC-MS (EI), and quantified using GC (FID) with the following the temperature program: initial temperature, 50 °C; heating rate 10 °C min^{-1} to 130 °C then increasing at a rate of 2 °C min^{-1} to 160 °C and then increasing at a rate of 5 °C min^{-1} to a final temperature of 250 °C; FID temperature, 280 °C. GC-MS analysis was performed under conditions identical to those used for GC analysis. Retention times: 14.8 min for **9** and 17.0 min for **8**.

3,5-Di-tert-butyl-5-(2-oxo-2-piperidinylethyl)-5H-furanone (6). GC-MS (EI) data found for $C_{19}H_{31}NO_3$, *m*/*z*, 321; ^1H NMR (200 MHz, $CDCl_3$): δ 1.10 (s, 9H), 1.21 (s, 9H), 1.54 (m, 6H), 2.90 and 3.06 (2H), 3.40 (m, 4H), 7.14 (s, 1H), and the GC-MS, ^1H NMR data were in agreement with literature data.

3,5-Di-tert-butyl-2-pyrone (8). GC-MS (EI) data found for $C_{13}H_{20}O_2$, *m*/*z*, 208 (M^+). ^1H NMR (200 MHz, $CDCl_3$): δ 1.17 (s, 9H), 1.35 (s, 9H), 7.08 (d, 1H), 7.14 (d, 1H).

4,6-Di-tert-butyl-2-pyrone (9). GC-MS (EI) data found for $C_{13}H_{20}O_2$, *m*/*z*, 208. ^1H NMR (200 MHz, $CDCl_3$): δ 1.19 (s, 9H), 1.26 (s, 9H), 6.15 (d, 1H).

Physical Measurements. Elemental analyses were performed on a Perkin-Elmer Series II CHNS/O Analyzer 2400. ^1H NMR spectra were recorded on a Bruker 200 MHz NMR spectrometer. The electronic spectra were recorded on Agilent diode array-8453 spectrophotometer. The Electron Paramagnetic Resonance (EPR) spectra were recorded on a JEOL JES-TE 100 and Varian X-band spectrometer. Mass spectrometry was performed on a QTOF and Thermo Finnigan LCQ 6000 Advantage Max ESI-MS spectrometer. Cyclic voltammetry (CV) and differential pulse voltammetry (DPV) were performed using a three electrode cell configuration. A platinum sphere, a platinum plate and Ag(s)/Ag^+ were used as working, auxiliary, and reference electrodes, respectively. The supporting electrolyte used was Bu_4ClO_4 (TBAP). The temperature of the electrochemical cell was maintained at 25.0 ± 0.2 °C by a cryocirculator (HAAKE D8 G). By bubbling research grade nitrogen, the solutions were deoxygenated and maintained an atmosphere of nitrogen over the solutions during measurements. The $E_{1/2}$ values were observed under identical conditions for various scan rates. The instruments utilized included an EG & G PAR 273 Potentiostat/Galvanostat and a Pentium-IV computer along with EG & G M270 software to carry out the experiments and to acquire the data. The product analysis was performed using an HP 6890 GC series gas chromatograph equipped with a FID detector and an HP-5 capillary column (30 m × 0.32 mm × 2.5 μm), and GC-MS analysis was performed on a Perkin-Elmer Clarus 500 GC-MS instrument using a PE-5 column.

Single-Crystal X-Ray Data Collection and Structure Solution. A suitable crystal of **1a** was mounted as a dark brown rod. The intensity data were collected at 173 K on a Stoe Mark II-Image Plate Diffraction System[49] equipped with a two-circle goniometer and using Mo Kα graphite monochromated radiation. Image plate distance 135 mm, ω rotation scans 0−180° at ϕ 0°, and 0−56° at ϕ 90°, step $\Delta\omega = 2.0°$, exposures of 6 min per image, 2θ range 1.70−51.55°, $d_{min} - d_{max} = 23.995 - 0.817$ Å. The structure was solved by Direct methods using the program SHELXS-97.[50] The refinement and all further calculations were carried out using SHELXL-97.[51] The H-atoms were included in calculated positions and treated as riding atoms using SHELXL default parameters. The non-H atoms were refined anisotropically, using weighted full-matrix least-squares on F^2. An empirical absorption correction was applied using the DELrefABS routine in PLATON;[52] transmission factors: $T_{min}/T_{max} = 0.579/0.872$. The crystallographic data are collected in Table 1.

Table 1. Crystal Data and Structure Refinement for $[Fe(L1)(TCC)]ClO_4$ **1a**

empirical formula	$C_{23}\ H_{22}\ Cl_5\ Fe\ N_4\ O_6$
fw	683.56
crystal system	monoclinic
space group	*P*21/*c*
a (Å)	8.8148(11)
b (Å)	16.0344(19)
c (Å)	18.993(3)
α (deg)	90
β (deg)	102.337(11)
γ (deg)	90
V (Å^3)	2622.5(6)
T (K)	173
Mo Kα λ, (Å)	0.71073
density (Mg m^{-3})	1.731
Z	4
μ (mm^{-1})	1.134
F(000)	1388
no. of reflections collected	21563
goodness-of-fit on F^2	0.859
R1[a]	0.0375
wR2[b]	0.0703

[a] $R1 = \Sigma||F_o| - |F_c||/\Sigma|F_o|$. [b] $wR2 = \Sigma w[(F_o^2 - F_c^2)^2/\Sigma w[(F_o^2)^2]\}^{1/2}$.

Results and Discussion

Synthesis and Characterization of Ligands and Complexes. The present ligands (Scheme 2) were synthesized according to known procedures[53] with suitable modifications, which involve reductive amination and simple substitution reactions. The cyclic diamine homopiperazine has been used as the starting material and its amino hydrogens have been replaced with differently substituted pyridylmethyl moieties to generate the ligands. The tetradentate ligands L1 and L2 were synthesized by reductive amination of pyridine carboxaldehyde and 6-methylpyridinecarboxaldehyde, respectively, using sodium triacetoxyborohydride as the reducing agent. The ligand L3 containing a quinolyl moiety was prepared by reacting homopiperazine with 2 equiv each of 2-chloromethylquinoline and Et_3N. The bis(pyridylmethyl) moieties of the 4N ligands mimic the metal coordinating imidazole moiety of the histidine amino acid side chain in dioxygenase enzymes. The pyridyl and sterically hindering 6-methylpyridyl/quinolyl moieties [pK_a (BH^+): pyridine, 5.2; quinoline, 4.94] in the ligands are expected to influence the coordination structures as well as the electronic properties and reactivity of the iron(III) model complexes. The iron(III) complexes (**1**−**4**) of the neutral ligands **L1**−**L4** with the general formula $[Fe(L)Cl_2]^+$ were generated in situ by the stoichiometric reaction of $FeCl_3$ with the ligands **L1**−**L4**. All the new complexes were characterized by ESI-MS,

(49) *X-Area V1.17 & X-RED32 V1.04 Software*; Stoe & Cie GmbH: Darmstadt, Germany, 2002.
(50) Sheldrick, G. M. *Acta Crystallogr.* **1990**, *A46*, 467–473; SHELXS-97 Program for Crystal Structure Determination.
(51) Sheldrick, G. *SHELXL-9*; Universität Göttingen: Göttingen, Germany, 1999.
(52) Spek, A. L. *J. Appl. Crystallogr.* **2003**, *36*, 7–13.
(53) Abdel-Magid, A. F.; Carson, K. G.; Harris, B. D.; Maryanoff, C. A.; Shah, R. D. *J. Org. Chem.* **1996**, *61*, 3849–3862.

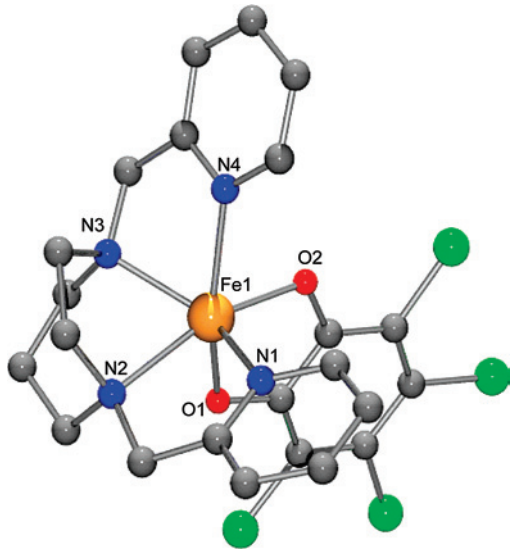

Figure 1. Molecular structure of the complex cation of [Fe(L1)(TCC)](ClO_4) **1a** (40% probability factor for the thermal ellipsoid). Hydrogen atoms have been omitted for clarity.

Table 2. Selected Bond Lengths [Å] and Bond Angles (°) for [Fe(L1)(TCC)]ClO_4 **1a**

Fe(1)−O(1)	1.940(2)
Fe(1)−(O2)	1.967(2)
Fe(1)−N(1)	2.104(3)
Fe(1)−N(2)	2.245(3)
Fe(1)−N(3)	2.145(3)
Fe(1)−N(4)	2.249(3)
O(1)−Fe(1)−O(2)	81.53(10)
O(1)−Fe(1)−N(1)	99.51(10)
O(1)−Fe(1)−N(2)	83.03(11)
O(1)−Fe(1)−N(3)	104.91(10)
O(1)−Fe(1)−N(4)	155.79(11)
O(2)−Fe(1)−N(1)	98.22(10)
O(2)−Fe(1)−N(2)	163.08(9)
O(2)−Fe(1)−N(3)	118.69(10)
O(2)−Fe(1)−N(4)	78.41(9)
N(1)−Fe(1)−N(2)	77.55(11)
N(1)−Fe(1)−N(3)	137.95(11)
N(1)−Fe(1)−N(4)	96.64(11)
N(2)−Fe(1)−N(3)	72.15(10)
N(2)−Fe(1)−N(4)	118.19(10)
N(3)−Fe(1)−N(4)	73.70(10)

electronic, and EPR spectral and electrochemical techniques. The iron(III)-catecholate complexes [Fe(L1)(TCC)]ClO_4 **1a**, [Fe(L2)(TCC)]ClO_4 **2a**, and [Fe(L3)(TCC)]NO_3 **3a** were prepared from $Fe(ClO_4)_3 \cdot xH_2O$ and $Fe(NO_3)_3 \cdot 9H_2O$, respectively, and the corresponding ligand by using similar synthetic routes. The treatment of the complexes generated in solution with 1 equiv of TCC^{2-} changed the solution from yellow-red to dark purple because of the TCC^{2-}-to-iron(III) charge transfer transition appearing around 580 nm. The di-*tert*-butylcatecholate ($HDBC^-$/DBC^{2-}) adducts of the iron(III) complexes were generated in solution for spectral and reactivity studies.

Description of the Crystal Structure of [Fe(L1)(TCC)](ClO_4) 1a. The molecular structure of complex **1a** is shown in Figure 1 together with the atom numbering scheme, and the selected bond lengths and bond angles are collected in Table 2. The complex cation possesses a distorted octahedral coordination geometry around iron(III). The two tertiary amine and two pyridyl nitrogen atoms of

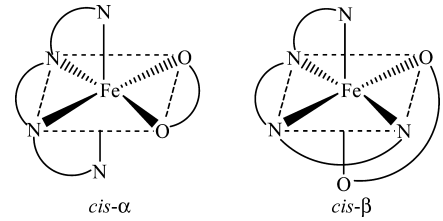

Figure 2. Illustration of different configurations adopted by the tetradentate N donor ligands in the catecholate adducts.

the tetradentate 4N ligand occupy four coordination sites of iron(III) in a cis-β rather than cis-α configuration (Figure 2) and the two oxygen atoms of tetrachlorocatecholate ion occupy the remaining cis positions. The Fe−$N1_{py}$ bond (2.104 Å) is shorter than the Fe−$N3_{amine}$ bond because of sp^2 and sp^3 hybridizations, respectively, of the pyridyl and tertiary amine nitrogen atoms.[30,43,54,55] However, the Fe−$N4_{py}$ bond (2.249 Å) is longer than the Fe−$N1_{py}$ bond (2.104 Å), and the Fe−$N2_{amine}$ bond (2.245 Å) is also longer than the other Fe−$N3_{amine}$ (2.145 Å) bond. This is obviously due to the trans effect exerted by the strongly bound catecholate oxygen donor atoms, supported by the buckling of the cyclic diamine backbone. Further, the Fe−O_{cat} bond lengths (1.940, 1.967 Å) are slightly asymmetric differing by 0.027 Å only. The bond angles N1−Fe1−N3 (137.95°), O2−Fe1−N2 (163.08°) and O1−Fe1−N4 (155.79°) and the bond angles O2−Fe1−N1 (98.22°), O2−Fe1−N4 (78.41°), N3−Fe1−N4 (73.70°), N2−Fe1−N3 (72.15°), O1−Fe1−N2 (83.03°), and O1−Fe1−N1 (99.51°) deviate respectively from the ideal octahedral angles of 180° and 90° revealing significant distortion in the coordination sphere. It is interesting that the cis-β configuration of **1a** is in contrast to the cis-α configuration[47] of the analogous complex [Fe(L4)(DBC)]$^+$. Obviously, the steric constraints of the cyclic diamine backbone of L1 do not appear to facilitate the disposition of the pyridylmethyl arms in trans positions and support the cis-α configuration.

Electronic Absorption and EPR Spectra. The electronic absorption spectra of [Fe(L)Cl_2]$^+$ **1**−**4** in acetonitrile solution exhibit two intense bands around 315 and 360 nm (Table 3), which arise from $Cl^- \rightarrow$ Fe(III) ligand-to-metal charge transfer (LMCT) transition.[27c,30] The more intense bands below 250 nm are caused by $\pi \rightarrow \pi^*$ transitions within the ligands. When H_2DBC pretreated with 1 equiv of Et_3N is added to **1**−**3** in acetonitrile only one catecholate-to-iron(III) LMCT band[26–35,43,46] (648−800 nm, Figure 3) appears. This is in contrast to the observation of two catecholate-to-iron(III) LMCT bands (927, 552 nm) for **4** upon its treatment with H_2DBC pretreated with 1 equiv of Et_3N in the present study (Figure 4). However, two visible bands (523−565, 820−832 nm, Table 3, Figure 3) appear upon adding H_2DBC pretreated with 2 equiv of Et_3N to **1**−**3** in acetonitrile solution, and they are assignable to DBC^{2-}-to-Fe(III) LMCT transitions[26–35,43,46] involving two different catecholate orbitals on the chelated DBC^{2-}. Also, when H_2DBC pretreated with

(54) Thomas, K. R. J.; Velusamy, M.; Palaniandavar, P. *Acta Crystallogr.* **1998**, *C54*, 741–743.
(55) Rodriguez, M. C.; Lambert, F.; Morgenstern-Badarau, I.; Cesario, M.; Guilhem, J.; Keita, B.; Nadjo, L. *Inorg. Chem.* **1997**, *36*, 3525–3531.

Table 3. Electronic Spectral Data for Iron(III) Complexes[a] and Their Catecholate Adducts in Acetonitrile Solution

added catechols[b]	λ_{max}, nm (ε, M^{-1} cm^{-1})			
	$[Fe(L1)Cl_2]^+$	$[Fe(L2)Cl_2]^+$	$[Fe(L3)Cl_2]^+$	$[Fe(L4)Cl_2]^+$
none	357 (2 220)	354 (10 980)	359 (10 820)	363 (4 220)
	314 (3 290)	317 (14 040)	317 (19 610)	293 (6 780)
H_2DBC[c]	726 (1 320)	648 (1 860)	800 (1 730)	927 (500)
	330 (sh)	335 (sh)	467 (1 680)	552 (390)
	288 (9 370)	270 (13 300)	316 (12 140)	393 (850)
H_2DBC	832 (2 290)	820 (1 950)	826 (1 880)	927 (1 000)
	565 (1 610)	523 (1 520)	529 (1 490)	552 (724)
	360 (13 610)	357 (7 420)	357 (8 640)	393 (1 850)
	308 (15 390)	310 (9 820)		283 (5 220)
H_2DBC[d]	762 (1 890)	642 (1 980)	807 (1 920)	924 (1 470)
	578 (1 740)	422 (1 840)	469 (1 890)	551 (1 040)
	337 (sh)	271 (12 180)	316 (11 990)	397 (1 500)
	283 (8 890)			
H_2TBC	718 (1 770)	526 (2 290)	546 (1 940)	903 (1 330)
	544 (1 850)	333 (sh)	349 (sh)	524 (960)
	343 (2 700)	288 (8 470)	316 (12 360)	339 (2 200)
	288 (8 110)	267 (11 700)		285 (5 860)
H_2TCC	585 (2 010)	579 (2 230)	569 (2 360)	563 (1 850)
	303 (7 320)	362 (sh)	315 (2 1470)	362 (sh)
	253 (15 330)	300 (7 740)		
H_2PCA	640 (3 628)	591 (3 020)	582 (3 070)	770 (1 610)
	322 (9 810)	311 (10 090)	376 (5 900)	488 (1 600)
	251 (14 020)			366 (sh)

[a] Generated by the reaction of ligands with ferric chloride (2×10^{-4} M). [b] The ratio of added ligand to iron(III) complexes was 1:1; the anions were generated by adding 2 equiv of triethylamine. [c] $HDBC^-$ was generated by adding 1 equiv of triethylamine. [d] DBC^{2-} was generated by adding 2 equiv of piperidine.

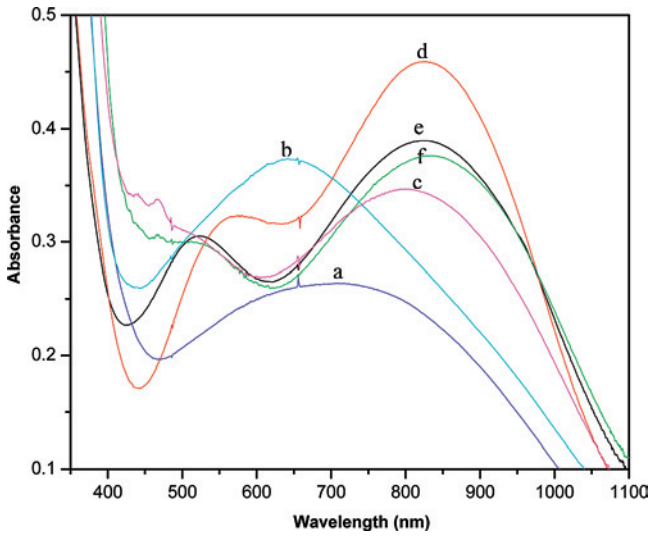

Figure 3. Electronic absorption spectra of iron(III) complex-HDBC or complex-DBC adducts (2.0×10^{-4} M) generated in situ by treating complexes with $HDBC^-$ (1 equiv of Et_3N) or DBC^{2-} (2 equiv of Et_3N). $[Fe(L1)(HDBC)]^{2+}$ (a); $[Fe(L2)(HDBC)]^{2+}$ (b); $Fe(L3)(HDBC)]^{2+}$ (c); $[Fe(L1)(DBC)]^+$ (d); $Fe(L2)(DBC)]^+$ (e); $Fe(L3)(DBC)]^+$ (f).

1 or 2 equiv of piperidine as base is added to **1**−**3** in acetonitrile, two DBC^{2-}-to-iron(III) LMCT bands (422−578, 642−807) are displayed. All these observations reveal that the adducts $[Fe(L)(DBC)]^+$ of complexes **1**−**4** are generated in situ in acetonitrile when H_2DBC is pretreated with 2 equiv of Et_3N or piperidine while the adducts $[Fe(L)(HDBC)]^{2+}$ are generated[46] in situ when H_2DBC is pretreated with only 1 equiv of the weaker base Et_3N (Figure 4). To throw light on the effect of the base on the nature of the catecholate adduct formed, spectrophotometric and pH titrations were performed (Supporting Information, Figures S3, S4). An acetonitrile solution containing a mixture of 1 equiv each of $[Fe(L3)Cl_2]^+$ and H_2DBC is titrated with Et_3N or piperidine, and the titration monitored by following the changes in pH and the catecholate-to-iron(III) LMCT band. When the base is added, the catecholate-to-iron(III) LMCT band around 800 nm (cf. above) increases in absorbance and then remains constant. Also, the high energy catecholate-to-iron(III) LMCT band starts developing around 530 nm and ∼2.0 equiv of Et_3N or piperidine are needed for the deprotonation. The pK_a value of iron(III) bound $HBDC^-$ is estimated as ∼4.3 (Et_3N) and ∼4.4 (piperidine) from the half-neutralization point, and a higher amount of Et_3N base is needed for the neutralization. So, it is evident that the actual complex species present in solution is $[Fe(L3)(HDBC)]^{2+}$ (Scheme 3) with bidentate coordination of $HDBC^-$. The spectrophotometric titration of **4** reveals that 2 equiv of Et_3N or piperidine are needed for the deprotonation of the iron(III) bound catechol. In contrast to **3**, two end points (pK_a, ∼ 2.9, 3.5) are discerned for the titration of the catechol adduct of **4** with Et_3N. However, only one neutralization point is detected (pK_a, 3.5) when piperidine is used as base. All these observations are consistent with the complex **4** forming the adduct $[Fe(L4)(H_2DBC)]^{3+}$ in which both the catechol protons are bound but more weakly than that in $[Fe(L3)(HDBC)]^{2+}$. Structural evidence for the bidentate coordination of monoanionic $HDBC^-$ in $[Fe(6\text{-}Me_3TPA)(HDBC)]^+$ and $[Fe(6\text{-}Me_2BPMCN)(HDBC)]^+$ have been obtained by Que. et al.[44] Further, the complex **1** has been proposed to have the tetradentate ligand occupy four equatorial sites of the iron(III) center and chloride ions occupy two labile sites trans to each other.[56] So it is interesting that upon adding the catecholate dianion to $[Fe(L)Cl_2]^+$ **1**−**3**, the sterically constrained linear tetradentate ligands **L1**−**L3** rearrange themselves to provide cis-coordination positions for bidentate coordination of the catecholate, as revealed in the X-ray structure of **1a**.

The energies of the DBC^{2-}-to-Fe(III) LMCT bands of the adducts $[Fe(L)(HDBC)]^{2+}$ and $[Fe(L)(DBC)]^+$ show a remarkable dependence on the nature of the primary ligands[27−33] **L1**−**L3**: $[Fe(L2)(DBC)]^+ > [Fe(L3)(DBC)]^+ > [Fe(L1)(DBC)]^+$. The increase in energies of the bands reflects the decrease in Lewis acidity of the iron(III) center of the adduct along the above series, as modified[29,33,36] by the replacement of the pyridylmethyl arm (**1**) by the (6-methyl)pyridylmethyl (**2**) and quinolylmethyl (**3**) arms. Thus, as the 6-methyl group is incorporated on the pyridyl ring in $[Fe(L1)(DBC)]^+$, the lone pair orbital on the pyridyl nitrogen is not oriented exactly toward the iron(III) orbital, the negative charge built on iron(III) decreases, and, as a result, the dπ* orbitals of iron(III) stabilized[36,43] leading to an increase in energy gap between the dπ* orbital and the ligand orbital and hence the observed increase in the LMCT band energies. Further, the adducts $[Fe(L1)(TBC)]^+$ (544, 718 nm) and $[Fe(L4)(TBC)]^+$ (524, 903 nm) also exhibit two visible bands but, interestingly, $[Fe(L2)(TBC)]^+$ (526 nm) and $[Fe(L3)(TBC)]^+$ (546 nm) display only one band

(56) Chen, K.; Que, L., Jr *Angew. Chem., Int. Ed.* **1999**, *38*, 2227–2229.

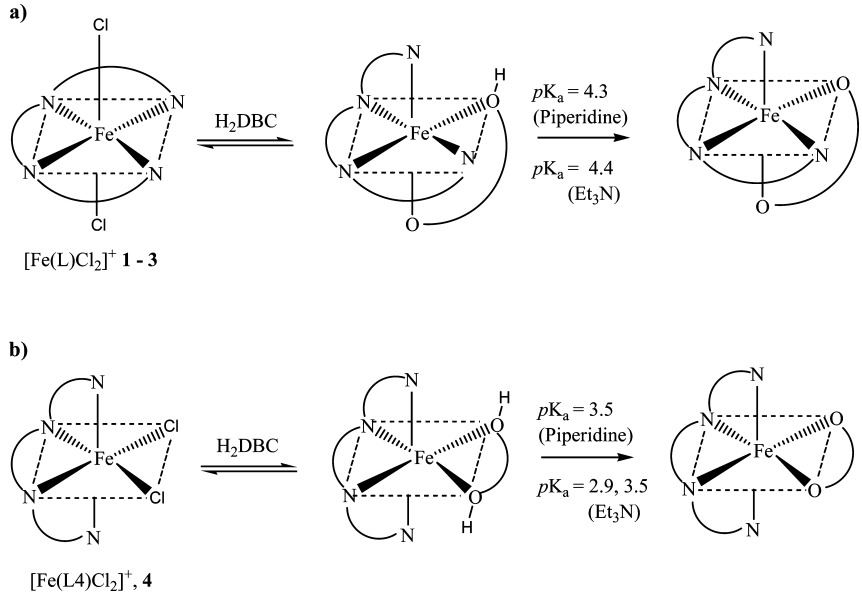

Figure 4. Schematic illustration of *cis*-β (a) and *cis*-α (b) coordination of DBC^{2-} to iron(III) center.

Scheme 3

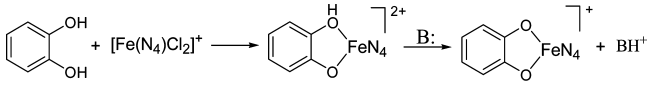

(a)

suggesting bidentate coordination of the dianionic catecholate containing sterically hindering *tert*-butyl substituent to iron(III) coordinated already to 4N ligands with sterically hindering 6-Me and quinolyl moieties, respectively. However, in contrast to these adducts, only one catecholate-to-Fe(III) LMCT band (569−640 nm) appears on adding TCC^{2-} and PCA^{2-} to the complex species **1**−**3** in acetonitrile solution suggesting the merger of both the low and high energy bands expected of the weaker coordination of TCC^{2-} and PCA^{2-} as expected. However, interestingly, the adduct $[Fe(L4)(PCA)]^+$ exhibits two visible bands (488, 770 nm) suggesting the absence of any steric hindrance to adduct formation.

The position of the low energy catecholate → Fe(III) LMCT band in the complex-substrate adducts [Fe(L1)(catecholate)] generated from $[Fe(L1)Cl_2]^+$ with no steric hindrance on the pyridyl moiety is found to be shifted to higher energies as the substituents[27–33,36] on the catecholate ring are varied from electron-releasing to electron-withdrawing as observed[29,30,44] previously: DBC^{2-} (832 nm) > TBC^{2-} (718 nm) > PCA^{2-} (640 nm) > TCC^{2-} (585 nm) (Table 3). This is expected as the electron-releasing substituents on the catecholate ring would decrease while electron-withdrawing substituents enhance the energy of the low energy band,[27–33] thus reflecting the importance of electronic effects expressed by the substituents on catechols. In contrast to the L1 adduct, the order of energy for the adducts $[Fe(L2)(catecholate)]^+$ and $[Fe(L3)(catecholate)]^+$ is TBC^{2-} > TCC^{2-} > PCA^{2-} > DBC^{2-}; this illustrates the importance of steric demand of 6-Me substituent on pyridyl rings and quinolyl moieties on the extent of catecholate adduct formation.

Table 4. EPR Spectral Data for Iron(III) Complexes and Their TCC^{2-} Adducts in Methanol/Acetone Solution at 77 K

compound	*g* values	*E/D*
$[Fe(L1)Cl_2]^+$ **1**	7.86, 4.0, 2.12 4.40[a], 2.06, 1.94, 1.89, 1.83	0.080
$[Fe(L1)(TCC)]ClO_4$ **1a**	8.50, 4.20, 2.10 4.9[a], 2.01, 1.99, 1.93, 1.88	0.090
$[Fe(L2)Cl_2]^+$ **2**	7.63, 4.05, 2.11 4.61[a], 2.05, 1.98, 1.88, 1.84	0.075
$[Fe(L2)(TCC)]ClO_4$ **2**a	8.1, 4.2, 2.1 5.1[a], 2.02, 2.0, 1.93, 1.87	0.085
$[Fe(L3)Cl_2]^+$ **3**	8.04, 4.02, 2.10 4.78[a], 2.06, 1.96, 1.88, 1.83	0.083
$[Fe(L3)(TCC)]NO_3$ **3a**	8.40, 4.10, 2.10 5.0[a], 2.0, 1.98, 1.93, 1.87	0.089

[a] Minor component.

The frozen solution EPR spectra of all the complexes are dependent on the substituents on the pyridyl moieties. The EPR spectrum of **1** (Supporting Information, Figure S1, Table 4) displays high-spin ($S = 5/2$) rhombic ferric signals[35,57] at $g = 7.9$, 4.0, and 2.1 (*E/D*, 0.080), which are associated with the $|5/2, -1/2\rangle \rightarrow |5/2, +1/2\rangle$ transition and also signals corresponding to rhombic low-spin[57,58] ($S = 1/2$) iron(III) species (g, 4.40, 2.06, 1.94, 1.89, 1.83). Upon replacing the pyridyl arms as in **1** by the sterically hindering 6-Me-pyridyl arms as in **2** and by the bulky and weakly σ-bonding quinolyl arms as in **3**, similar high-spin ferric signals are observed but with shifts in *g* values and changes in *E*/*D* values (**2**: 7.6, 4.1, 2.1, *E/D*, 0.075; **3**: 8.0, 4.0, 2.1, *E/D*, 0.083) (Supporting Information, Figure S2, Table 4) suggesting differences in rhombicity of the iron(III) coordination sphere. Further, the TCC^{2-} adducts of complexes **1**−**3** also exhibit similar rhombic ferric signals but with large shifts in *g* values

(57) (a) Fujii, H.; Funabashi, Y. *Angew. Chem., Int. Ed.* **2002**, *41*, 3638–3641. (b) Kurahashi, T.; Kobayashi, Y.; Nagatomo, S.; Tosha, T.; Kitagawa, T.; Fujii, H. *Inorg. Chem.* **2005**, *44*, 8156–8166. (c) Kurahashi, T.; Oda, K.; Sugimoto, M.; Ogura, T.; Fujii, H. *Inorg. Chem.* **2006**, *45*, 7709–7721.

(58) (a) Simaan, A. J.; Biollot, M.-L.; Riviere, E.; Boussac, A.; Girerd, J. -J. *Angew. Chem., Int. Ed.* **2000**, *39*, 196–198. (b) Bukowshi, M. R.; Comba, P.; Limberg, C.; Merz, M.; Que, L., Jr.; Wistuba, T. *Angew. Chem., Int. Ed.* **2004**, *43*, 1283–1287.

Table 5. Electrochemical Data[a] for Fe^{III}/Fe^{II} Redox Process of Iron(III) Complexes and Their DBC^{2-} Adduct Generated Using Et_3N in Acetonitrile at 25 ± 0.2 °C and a Scan Rate of 5 mV/s (DPV)

	$E_{1/2}$ (V)	
compound	Fe^{III}/Fe^{II}	DBSQ/H_2DBC
$[Fe(L1)Cl_2]^+$	−0.282	
+ H_2DBC	−0.285	
+ $HDBC^-$	−0.299	0.061
+ DBC^{2-}	−0.863[b]	0.049
+ $HDBC^-$[c]	−0.701	−0.089
+ DBC^{2-}[c]	−0.703	−0.079
$[Fe(L2)Cl_2]^+$	−0.305	
+ H_2DBC	−0.271	
+ $HDBC^-$	−0.295	0.027
+ DBC^{2-}	−0.325	0.051
+ $HDBC^-$[c]	−0.249	0.057
+ DBC^{2-}[c]	−0.657	−0.065
$[Fe(L3)Cl_2]^+$	−0.310	
+ H_2DBC	−0.303	
+ $HDBC^-$	−0.315	0.031
+ DBC^{2-}	−1.117[b]	0.165
+ DBC^{2-}[c]	−1.037	−0.077
$[Fe(L4)Cl_2]^+$	−0.125	
+ H_2DBC	−0.123	
+ DBC^{2-}	−0.119	−0.119

[a] Potential measured vs $Ag/AgNO_3$ (0.01 M, 0.1 M TBAP); add 0.544 V to convert to NHE. [b] Ligand reduction. [c] Generated by adding 2 equiv piperidine to H_2DBC.

(**1a**: 8.5, 4.2, 2.1, *E/D*, 0.090; **2a**: 8.1, 4.2, 2.1, *E/D*, 0.085; **3a**: 8.4, 4.1, 2.1, *E/D*, 0.089). The increase in *E/D* value upon adding TCC^{2-} reveals that considerable distortion occurs in the coordination sphere of iron(III) centers in **1**−**3** upon coordination of TCC^{2-}.

Electrochemical Behavior. The redox behavior of the iron(III) complexes and their catecholate adducts generated in situ in acetonitrile solution was studied on a stationary platinum sphere electrode by employing CV and DPV. The complexes **1**−**4** exhibit a cathodic (−0.160 to −0.390 V) as well as an anodic wave (−0.088 to −0.260 V, Supporting Information, Table S1). The cathodic current functions (D, $1.0-3.6 \times 10^{-6}$ cm^2/sec) calculated by substituting the slope obtained from the linear i_{pc} vs $\nu^{1/2}$ ($\nu < 0.05$ V s^{-1}) plot in the Randles−Sevcik equation[59] are of the same order as those observed for other iron(III) complexes undergoing a one-electron reduction process.[27–30,43,46] The $E_{1/2}$ values of Fe^{III}/Fe^{II} redox potentials of the complexes from DPV (Table 5) vary in the order **4** > **1** > **2** ≥ **3** suggesting a decrease in Lewis acidity of the iron(III) center along this order. Obviously, the coordinated chloride ions compensate[43,46] for the increase in positive charge on iron(III) caused by the sterically hindering 6-methyl group and the less basic and bulky quinolyl arms. On addition of 1 equiv of H_2DBC to **1**, an intense reduction wave typical of DBSQ/$HDBC^-$ (DBSQ = di-*tert*-butylsemiquinone) couple of $[Fe(L1)(HDBC)]^{2+}$ (cf. above) species superimposed on the $Fe^{III} \rightarrow Fe^{II}$ reduction wave ($E_{1/2}$, −0.285 V) and a reduction wave characteristic of DBQ/DBSQ couple ($E_{1/2}$, 0.314 V) appear. Upon addition of 1 equiv of piperidine as base, the DBSQ/

(59) Bard, A. J.; Faulkner, L. R. *Electrochemical Methods: Fundamental and Applications*; John Wiley & Sons: New York, 1980; pp 218.

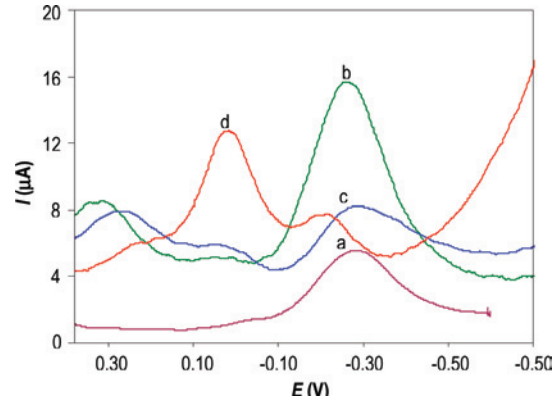

Figure 5. Differential pulse voltammograms of 1 mM $[Fe(L1)Cl_2]^+$ before (a) and after addition of 1 mM H_2DBC (b), 1 mM Et_3N (c), and 2 mM Et_3N (d) in acetonitrile at 25 °C. Supporting electrolyte, 0.1 M TBAP; scan rate, 5 mV s^{-1}; reference electrode, Ag/Ag^+; working electrode, Pt sphere.

$HDBC^-$ reduction wave of $[Fe(L1)(HDBC)]^{2+}$ adduct (cf. above) is shifted to a more positive potential ($E_{1/2}$, −0.089 V), the $Fe^{III} \rightarrow Fe^{II}$ reduction appears as a distinct wave at a more negative potential ($E_{1/2}$, −0.701 V), and the DBQ/DBSQ reduction wave[27–30,43,46] is shifted to a more positive potential ($E_{1/2}$, 0.487 V). On addition of one more equiv of piperidine, the peak current around −0.079 V increases suggesting the formation of more amount of the $[Fe(L1)(DBC)]^+$ adduct. Similar observations are made upon adding 1 and 2 equiv of Et_3N (Table 5, Figure 5); the DBSQ/DBC^{2-} couple appears around 0.061 V, and the $Fe^{III} \rightarrow Fe^{II}$ reduction peak ($E_{1/2}$, −0.299 V) of $[Fe(L1)Cl_2]^+$ still remains suggesting that the $[Fe(L1)(HDBC)]^{2+}$ species are in equilibrium with $[Fe(L1)Cl_2]^+$ species. The Fe^{III}/Fe^{II} redox couple of $[Fe(L1)(DBC)]^+$ adduct appears as a shoulder at a more negative redox potential because of chelation of DBC^{2-} on the ligand reduction peak ($E_{1/2}$, −0.863 V).[46] Similar observations are made for **1** and **2** also upon adding piperidine and Et_3N as base. The redox potential of coordinated DBSQ/$HDBC^-$ couple is located in the range 0.165 to −0.079 V, which is more positive than that of free DBSQ/DBC^{2-} couple (CH_3CN: −1.274 V) reflecting the significant stabilization of coordinated DBC^{2-} anion toward oxidation. Interestingly, the redox potentials fall in the same range as that observed for the DBC^{2-} adducts of iron(III) complexes of 3N ligands.[30,43] This illustrates that the reactivity of all these adducts are very similar because of the similarity in the iron(III) environments.

Upon addition of 1 equiv of H_2DBC to $[Fe(L4)Cl_2]^+$ **4**, no appreciable shift in the redox wave assigned to Fe^{III}/Fe^{II} couple is observed. On addition of 1 or 2 equiv of Et_3N, no change in this wave is observed but a new redox wave corresponding to DBQ/DBSQ redox couple[27–30] appears ($E_{1/2}$, 0.373 V, Table 5). It is evident that for the $[Fe(L4)(H_2DBC)]^{3+}$ species formed (cf. above) in the absence of the added base, the DBSQ/H_2DBC couple is located at a potential same as that for the Fe^{III}/Fe^{II} couple of the parent complex. This is in contrast to the observation of both the Fe(III)/Fe(II) as well as DBSQ/$HDBC^-$ redox waves for **1**−**3** upon adding H_2DBC and the increase in cathodic peak current of the latter upon adding a base. Also, interestingly,

Table 6. Kinetic Data for the Oxidative Cleavage of H_2DBC Catalyzed by Iron(III) Complexes with O_2 in Acetonitrile/DMF and the Cleavage Products Analyzed after 24 h (see Figure 6)

		cleavage products (%)[a]				
complex	solvent/base[b]	intradiol	extradiol	k_{obs} (10^{-4} s^{-1})	k_{O_2} (10^{-2} M^{-1} s^{-1})[c]	$t_{1/2}$ (h)[d]
$[Fe(L1)(HDBC)]^{2+}$	CH_3CN/Et_3N	3.7 (**5**)	34.6 (**8,9**)	13.49 ± 0.44	16.66 ± 0.54	0.14
$[Fe(L1)(DBC)]^{+}$	CH_3CN/Et_3N	5.7 (**5**)	23.5 (**8,9**)	2.99 ± 0.16	3.69 ± 0.20	0.64
$[Fe(L1)(DBC)]^{+}$	CH_3CN/Pip	12.9 (**5**)	5.6 (**8,9**)	15.02 ± 0.90	18.54 ± 1.11	0.13
$[Fe(L1)(DBC)]^{+}$	DMF/Et_3N	8.6 (**5**)	2.3 (**9**)	2.67 ± 0.32	5.50 ± 0.66	0.72
$[Fe(L2)(HDBC)]^{2+}$	CH_3CN/Et_3N	0.4 (**5**)	72.5 (**8,9**)	3.76 ± 0.07	4.65 ± 0.08	0.51
$[Fe(L2)(DBC)]^{+}$	CH_3CN/Et_3N	2.9 (**5**)	65.9 (**8,9**)	0.85 ± 0.04	1.11 ± 0.05	2.15
$[Fe(L2)(DBC)]^{+}$	CH_3CN/Pip	12.5 (**5,6**)	9.6 (**8,9**)	3.28 ± 0.18	2.90 ± 0.23	0.58
$[Fe(L2)(DBC)]^{+}$	DMF/Et_3N	23.5 (**5,7**)	5.3 (**9**)	1.40 ± 0.18	2.90 ± 0.38	1.37
$[Fe(L3)(HDBC)]^{2+}$	CH_3CN/Et_3N	1.5 (**5**)	85.5 (**8,9**)	1.58 ± 0.05	1.96 ± 0.58	1.21
$[Fe(L3)(DBC)]^{+}$	CH_3CN/Et_3N	1.3 (**5**)	58.1 (**8,9**)	2.31 ± 0.20	2.85 ± 0.24	0.83
$[Fe(L3)(DBC)]^{+}$	CH_3CN/Pip	29.5 (**6**)	16.0 (**8,9**)	1.55 ± 0.07	1.92 ± 0.89	1.24
$[Fe(L3)(DBC)]^{+}$	DMF/Et_3N	4.1 (**5**)	1.6 (**9**)	3.85 ± 0.66	7.92 ± 1.35	0.50
$[Fe(L4)(DBC)]^{+}$ [e]	DMF	90.0 (**5**)		0.81	2.6	
$[Fe(L4)(DBC)]^{+}$	CH_3CN/Et_3N	20.7 (**5**)		0.19 ± 0.01	0.24 ± 0.01	9.88

[a] Based on H_2DBC. [b] Pip = piperidine. [c] $k_{O_2} = k_{obs}/[O_2]$. [d] $t_{1/2} = 0.693/k_{obs}$. [e] Taken from reference 47.

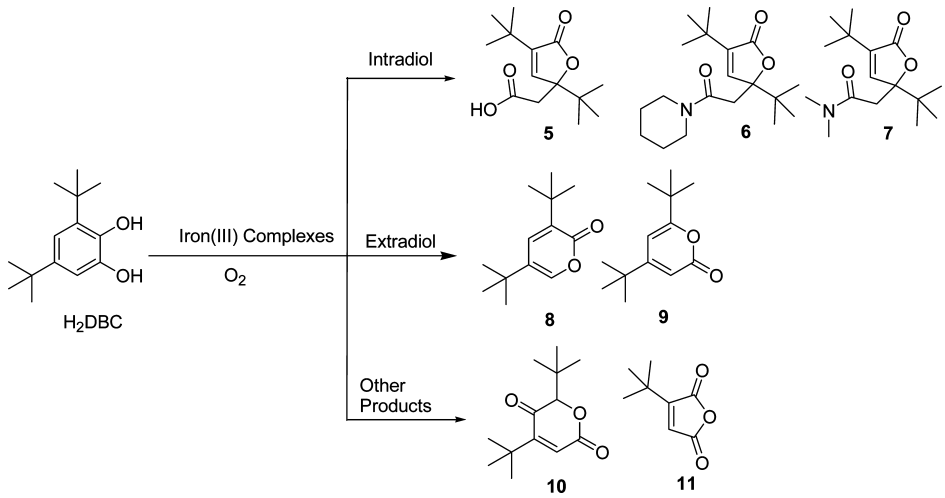

Figure 6. Oxygenation products of H_2DBC catalyzed by iron(III) complexes using dioxygen.

the $DBSQ/DBC^{2-}$ redox couple of $[Fe(L4)(DBC)]^{+}$ is located around −0.119 V, which is more negative than those for the corresponding L1−L3 adducts. This means that the electron transfer[23] from the catecholate adduct to dioxygen is thermodynamically less favorable in the L1−L3 adducts than in the L4 adduct.

Catechol Dioxygenase Activity of Iron(III) Complexes. The 3,5-di-*tert*-butyl-catecholate (DBC^{2-}) adducts were generated in situ in acetonitrile/DMF solution, and their reactivity toward O_2 was investigated by monitoring the decay of DBC^{2-}-to-iron(III) LMCT band. All the adducts were found to react with molecular oxygen, and the oxygenation reactions exhibit a pseudofirst order kinetics because of the excess of dioxygen used, as judged from the linearity of the plot of [1 + log(Absorbance)] versus time. The second order rate constants of the reactions were then calculated[27–30,43,47] using the equation $k_{O_2} = k_{obs}/[O_2]$ (Table 6), and the $t_{1/2}$ of the catecholate adducts were calculated[46] using the equation $t_{1/2} = 0.693/k_{obs}$. The oxygenation products were identified by GC-MS (EI) and ^{1}H NMR and quantified by GC (FID) techniques (Figure 6), and kinetic traces are provided in Figure 8 and Supporting Information, Figure S5.

When an acetonitrile solution of the adducts $[Fe(L)(HDBC)]^{2+}$ generated in situ (cf. above) by reacting the complexes **1**−**3** with H_2DBC pretreated with 1 equiv of Et_3N was exposed to excess of dioxygen, the intensity of the $HDBC^{-}$-to-iron(III) LMCT band decreased (Figure 7, Table 6, Supporting Information, Figure S5) with pseudofirst order kinetics (k_{obs}, 1.58−13.49 × 10^{-4} s^{-1}). The adducts $[Fe(L)(HDBC)]^{2+}$ of complexes **1**−**3** were reacted with dioxygen over 24 h ($t_{1/2}$: **1**, 0.14; **2**, 0.51; **3**, 1.21 h) to afford extradiol cleavage products (**1**, 34.6; **2**, 72.5; **3**, 85.5%) almost exclusively and intradiol products in very small amounts (**1**, 3.7; **2**, 0.4; **3**, 1.5%) (Figure 9, Table 6). The extradiol cleavage results in two isomeric products, di-*tert*-butyl-2-pyrones[38–41,60] $C_{13}H_{20}O_2$, *m*/*z*, 208, 3,5-di-*tert*-butyl-2-pyrone **8** (**1**, 21.3; **2**, 68.8; **3**, 80.9%) and 4,6-di-*tert*-butyl-2-pyrone **9** (**1**, 13.3; **2**, 3.7; **3**, 4.6%) with insertion of an oxygen atom into H_2DBC followed by loss[38,60] of CO. The intradiol cleavage product is $C_{15}H_{24}O_4$, *m*/*z*, 254, 3,5-di-*tert*-butyl-5-(carboxymethyl)-2-furanone **5** (**1**, 3.7; **2**, 0.4; **3**, 1.5%) and the side product is $C_{13}H_{19}O_3$, *m*/*z*, 223, 2,5-di-*tert*-butyl-2*H*-pyran-3,6-dione, **10** (**1**, 5.0; **2**, 1.0; **3**, 1.5%).

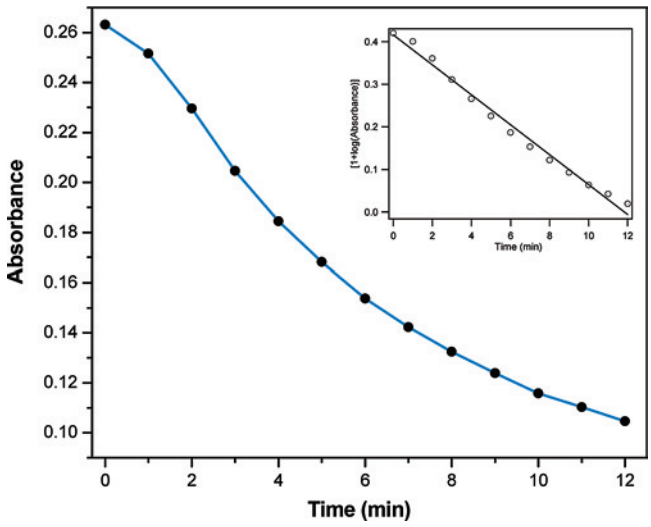

Figure 7. Progress of reaction for the reaction of $[Fe(L1)(HDBC)]^{2+}$ (2.0×10^{-4} M) with O_2 at 25 °C in acetonitrile solution. Inset**:** Plot of [1 + log(Absorbance)] vs time observed at 726 nm.

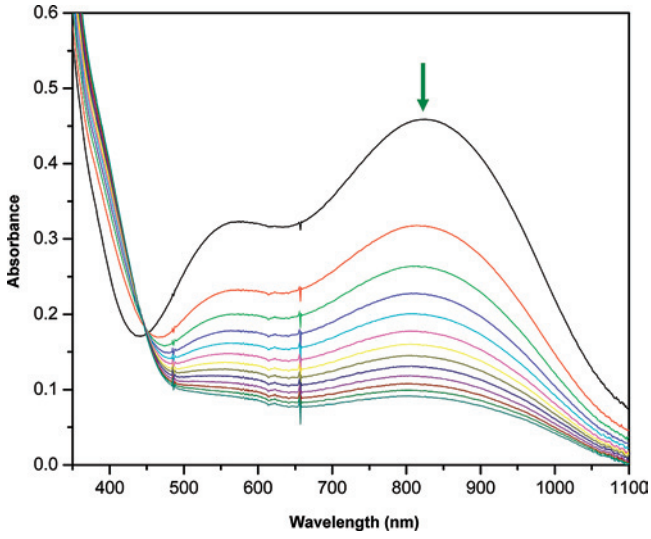

Figure 8. Progress of the reaction of $[Fe(L1)(DBC)]^{+}$ (2×10^{-4} M) with O_2 in acetonitrile solution; monitored disappearance of DBC^{2-}-to-Fe(III) LMCT band at 832 nm with 2.5 min time interval.

In contrast to $[Fe(L)(HDBC)]^{2+}$, the adducts $[Fe(L)(DBC)]^{+}$ generated in situ in acetonitrile solution (cf. above) by treating **1**−**3** with H_2DBC pretreated with 2 equiv of Et_3N show two distinct DBC^{2-}-to-iron(III) LMCT bands in the ranges 820−832 and 523−565 nm. Upon exposure of the adducts to excess of dioxygen, the decay of both the LMCT bands was observed (Figure 8, Table 6) to follow pseudofirst order kinetics (k_{obs}, $0.85-2.99 \times 10^{-4}$ s^{-1}). Upon reaction of the adducts $[Fe(L)(DBC)]^{+}$ in acetonitrile solution with excess of dioxygen over 24 h ($t_{1/2}$: **1**, 0.64; **2**, 2.15; **3**, 0.83 h) major amounts of the extradiol cleavage products **8** (**1**, 13.7; **2**, 61.7; **3**, 54.5%) and **9** (**1**, 9.8; **2**, 4.2; **3**, 3.6%), smaller amounts of the intradiol product **5** (**1**, 5.7; **2**, 2.9; **3**, 1.3%) and the side product **10** (**1**, 5.2; **2**, 1.0; **3**, 1.5%) were obtained.

For the adducts $[Fe(L)(DBC)]^{+}$ of complexes **1**−**3** generated in situ by reacting the complexes with H_2DBC pretreated with 2 equiv of piperidine as base in acetonirile solution, the two DBC^{2-}-to-iron(III) LMCT bands (642−807, 422−578 nm) were observed to disappear following pseudofirst order kinetics (k_{obs}, $1.55-15.02 \times 10^{-4}$ s^{-1}) on their exposure to excess of dioxygen. The product analysis after 24 h of reaction ($t_{1/2}$: **1**, 0.13; **2**, 0.58; **3**, 1.24 h) reveals a higher yield of the intradiol product **5** (**1**, 1.2; **2**, 2.5%) and $C_{19}H_{31}NO_3$, *m*/*z*, 321, 3,5-di-*tert*-butyl-5-(2-oxo-2-piperidinylethyl)-5*H*-furanone **6** (**1**, 11.7; **2**, 10.0; **3**, 29.5%) and a lower yield of the extradiol cleavage products **8** (**1**, 5.6; **2**, 6.3; **3**, 13.6%) and **9** (**1**, <1; **2**, 3.3; **3**, 2.4%). Further, the adducts generated in situ in DMF by treating the complexes with H_2DBC pretreated with 1 or 2 equiv of Et_3N show two distinct DBC^{2-}-to-iron(III) LMCT bands around 825 and 545 nm and undergo oxygenation on exposure to excess of dioxygen to afford only intradiol cleavage products **5** and 3,5-di-*tert*-butyl-5-(*N*,*N*-dimethylamidomethyl)-2-furanone **7** but with yields lower than those observed for the adducts generated in acetonitrile solution in the presence of piperidine as base.

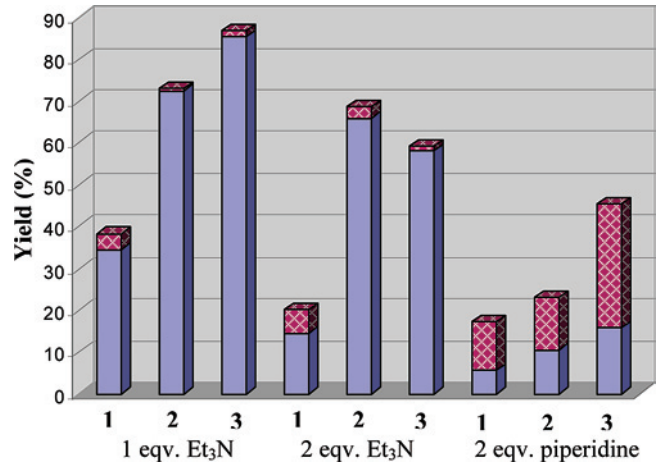

Figure 9. Base-dependent oxidative transformation of H_2DBC into intradiol (magenta) and extradiol (blue) cleavage products catalyzed by iron(III) complexes **1**−**3** using dioxygen.

It is remarkable that the adducts $[Fe(L)(HDBC)]^{2+}$ generated using 1 equiv of the weaker base Et_3N (pK_a (BH^+): 10.64) yield mainly extradiol cleavage products while the adducts $[Fe(L)(DBC)]^{+}$ generated using piperidine (pK_a (BH^+): 11.22) as base elicit intradiol cleavage products in higher amounts. We have already shown[46] that bidentate coordination of dianionic catecholate facilitates O_2 attack on the iron(III)-bound substrate to undergo intradiol cleavage while bidentate coordination of monoanionic catecholate favors extradiol cleavage. Also, the adduct $[Fe(L2)(HDBC)]^{2+}$ shows a higher extradiol to intradiol cleavage product selectivity (*E*/*I*, 181:1) than the other adducts $[Fe(L3)(HDBC)]^{2+}$ (*E*/*I*, 57:1) and $[Fe(L1)(HDBC)]^{2+}$ (*E*/*I*, 9:1) (Figure 9). As the adducts $[Fe(L)(HDBC)]^{2+}$ yield extradiol cleavage products almost exclusively, the trend in selectivity and the observed rates of cleavage may be illustrated by invoking the O_2 activation mechanism[23,37–41] for the extradiol cleavage (Scheme 4). Thus, on the basis of

(60) (a) Funabiki, T.; Mizoguchi, A.; Sugimoto, T.; Tada, S.; Tsuji, M.; Sakamoto, H.; Yoshida, S. *J. Am. Chem. Soc.* **1986**, *108*, 2921–2932. (b) Funabiki, T.; Mizoguchi, A.; Sugimoto, T.; Yoshida, S. *Chem. Lett.* **1983**, 917–920.

Scheme 4. Proposed Dioxygenation Reaction Mechanism for H_2DBC Catalyzed by **1**−**3** Using Dioxygen

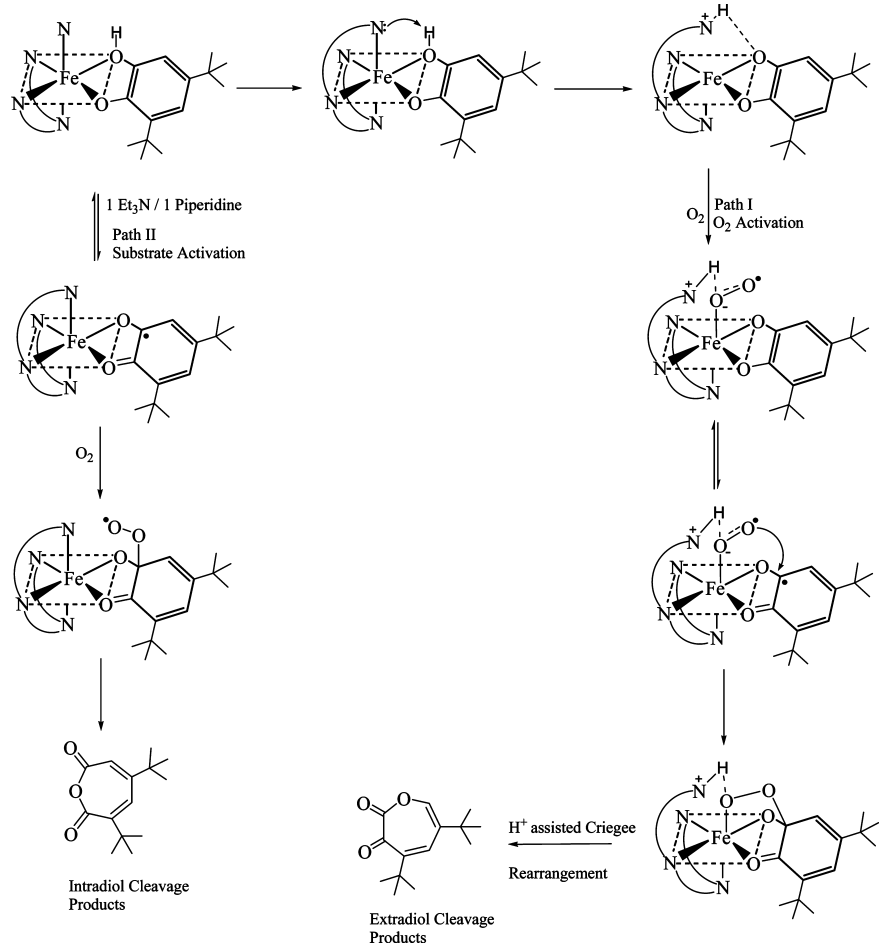

spectroscopic studies of extradiol dioxygenases, Lipscomb et al. have proposed that the simultaneous binding of substrate and O_2 to the iron allows transfer of electron density such that the substrate gains cation radical character while O_2 becomes a nascent superoxide.[61,62] It is remarkable that they have now established[23] the simultaneous presence of the key intermediates, the end-on O_2 adduct, the subtrate-alkylperoxo-Fe^{2+} intermediate, and the product complex in different subunits, in the X-ray crystal structure of the enzyme homoprotocatechuate 2,3-dioxygenase (2,3-HPCD) after its reaction with 4-nitrocatechol in the presence of dioxygen to give the extradiol cleavage product. So the X-ray crystal structure of the key hydroperoxo intermediate of 2,3-HPCD enzymes[23] and the previous analogue mechanistic studies[63,64] clearly imply the involvement of a proximal hydroperoxide intermediate. A similar reaction pathway and intermediate may be now invoked for illustrating the reactivity of the present iron(III) model reaction. Thus, the pyridyl arm located cis to both the catecholate oxygen atoms might act as an acid−base catalyst center (Scheme 4) as proposed for the extradiol cleaving enzymes.[63,64] Upon proton transfer to the pyridyl arm from the bound catecholate monoanion ($HDBC^-$), followed by weakening of its coordination to iron(III) and displacement from the coordination sphere of iron(III) center, the binding of O_2 to the iron(III) center occurs. The superoxide adduct $[Fe(L)(DBC)(O_2)]^+$ is then formed, and the bound superoxide with semiquinone radical rearranges to a proximal peroxy intermediate.[23,63,64] A concerted Criegee rearrangement of this intermediate mediated by the internal pyridinium salt formed earlier, leads to the formation of a seven-membered α-keto lactone as the extradiol cleavage product, which would proceed to form the observed pyrone or ring-opened product.[40,46] On the other hand, the O_2 molecule can also attack the catecholate-bound iron(III) and displace the other pyridyl nitrogen atom trans to one of the catecholate oxygen atoms. As the bound O_2 lies away from the enediolate moiety of catecholate, only the quinone would be elicited as the product.[39] As the product analysis (cf. above) reveals no quinone, such a pathway is ruled out.

The regiospecificity of the oxidative cleavage is thus determined by the nature and amount of base used and hence the site preferred for attack by molecular oxygen. The higher amounts of intradiol cleavage products observed for the $[Fe(L1)(HDBC)]^{2+}$ adduct are obviously due to the stronger binding of the pyridyl arm(s) to the iron(III) center with a

(61) Arciero, D. M.; Lipscomb, J. D. *J. Biol. Chem.* **1986**, *261*, 2170–2178.
(62) Shu, L.; Chiou, Y-M.; Orville, A. M.; Miller, M. A.; Lipscomb, J. D.; Que, L., Jr. *Biochemistry* **1995**, *34*, 6649–6659.
(63) Winfield, C. J.; Al-Mahrizy, Z.; Gravestock, M.; Bugg, T. D. H. *J. Chem. Soc., Perkin Trans. 1* **2000**, 3277–3289.
(64) Mendel, S.; Arndt, A.; Bugg, T. D. H. *Biochemistry* **2004**, *43*, 13390–13396.

Lewis acidity higher than the other two adducts (cf. above) and hence its decreased tendency to be substituted by dioxygen. The incorporation of the 6-Me group as in $[Fe(L2)(HDBC)]^{2+}$, though it encourages protonation, would hinder the approach of O_2 toward iron(III) causing a slower cleavage reaction. Similarly, the replacement of the pyridyl moiety in $[Fe(L1)(HDBC)]^{2+}$ by the bulkier quinolyl moiety as in $[Fe(L3)(HDBC)]^{2+}$ would also hinder the approach of molecular oxygen leading more to a still lower rate of cleavage. A similar dioxygenation activity for $[Fe(MeTPA)Cl_2]$[33] [MeTPA = (6-methylpyrid-2-ylmethyl)-bis(pyrid-2-ylmethyl)amine], $[Fe(BPQA)Cl_2]^+$ [BPQA = bis(2-pyridylmethyl)(2-quinolylmethyl)amine], and $[Fe(BQPA)Cl_2]^+$ [BQPA = bis(2-quinolylmethyl)(2-pyridylmethyl)amine], which is significantly lower than that for $[Fe(TPA)Cl_2]Cl$, has been previously observed.[26] Thus, electronic factors determine the selectivity of cleavage for the present catecholate adducts while both the steric and electronic factors determine the rates of cleavage reaction.

In contrast to $[Fe(L)(HDBC)]^{2+}$, the adducts $[Fe(L)(DBC)]^+$ generated by adding 1 or 2 equiv of piperidine display a lower extradiol cleavage selectivity and a different trend in selectivity (*E*/*I*: **1**, 0.4:1; **2**, 0.8:1; **3**, 0.5:1) (Figure 9). A stronger base like piperidine would facilitate the bidentate coordination of H_2DBC to form $[Fe(L)(DBC)]^+$ resulting in an increase in intradiol cleavage yield. The trend in the observed product selectivity and rates of catechol cleavage of $[Fe(L)(DBC)]^+$ complexes could be illustrated by invoking a substrate activation mechanism (Scheme 4) in which the rate determining step is O_2 attack on the substrate.[18,19,24–34,46] The direct attack of an O_2 molecule on the enediolate moiety of the semiquinone form of coordinated DBC^{2-} is followed by the peroxo coordination[23,26,38,46] to iron(III), which depends upon the availability of a coordination site. The weakly coordinated pyridyl ($Fe-N_{py}$, 2.249 Å) moiety of the sterically constrained **L1**−**L3** ligands is likely to be displaced, as quinone is elicited as the product leading to a regiospecific dioxygen activation. Subsequent decomposition of the resultant peroxide affords the intradiol cleavage product. The DBC^{2-} is bound in $[Fe(L2)(DBC)]^+$ more strongly than that in $[Fe(L3)(DBC)]^+$ because of the higher Lewis acidity of the iron(III) center, caused by the sterically hindered 6-methylpyridyl moiety (cf. above). This results in a lower tendency of the complex to displace the bound pyridyl nitrogen enabling dioxygen attack leading to extradiol cleavage to occur. Thus, the replacement of the pyridyl moiety as in $[Fe(L1)(DBC)]^+$ by the 6-methylpyridyl moiety as in $[Fe(L2)(DBC)]^+$ and that by the bulkier quinolyl moiety as in $[Fe(L3)(DBC)]^+$ would hinder the attack of O_2 on the chelated DBC^{2-} leading to, respectively, 6 and 9 times lower rate of dioxygenation of the substrate.

The product selectivities (*E*/*I*: **1**, 4:1; **2**, 23:1; **3**, 45:1) observed for $[Fe(L)(DBC)]^+$ generated in the presence of 2 equiv of Et_3N reveal that the yield of extradiol cleavage products are lower than those for their respective $[Fe(L)(HDBC)]^{2+}$ adducts but higher than those for the same adducts generated by using 2 equiv of piperidine. Also, the adduct $[Fe(L1)(DBC)]^+$ undergoes dioxygenation with a rate 5 times lower than that generated in the presence of piperidine. A larger proportion of the adducts is present as $[Fe(L)(HDBC)]^{2+}$ species (cf. spectral and electrochemical studies) in the presence of the weaker base used for deprotonation and so the extradiol cleavage pathway is mostly followed. The sterically highly demanding 6-Me group rather than the quinolyl moiety in these adducts appears to offer more steric hindrance to dioxygen attack on iron(III) leading to the decreased rate of extradiol cleavage to occur. Thus, all the present results reveal the importance of the steric demand of coordinated 6-methylpyridine and quinolyl moieties in fine-tuning the Lewis acidity and also offering steric hindrance to O_2 attack and hence the product selectivity as well as rates of dioxygenation.

The exclusive extradiol cleavage effected by the $[Fe(L)(DBC)]^+$ adducts of **1**−**3** is interesting because the analogous ethylenediamine-based adduct $[Fe(L4)(DBC)]^+$ has been reported[47] to afford the intradiol cleavage product **5** exclusively (90%) upon exposure to molecular oxygen. In the present study, the complex $[Fe(L4)Cl_2]^+$ displays two DBC^{2-}-to-iron(III) LMCT bands (Table 3) in acetonitrile solvent upon treatment with H_2DBC even in the presence of 1 equiv of the weaker base Et_3N and when treated with one more equiv of Et_3N the bands become more intense. This suggests that bidentate coordination of DBC^{2-}, facilitated by the higher Lewis acidity of the iron(III) center, leads to the *cis*-α configuration for the adduct. Also, the adduct $[Fe(L4)(DBC)]^+$ generated in the present study affords only a small amount of intradiol cleavage product **5** (20.7%) and the side product 3-*tert*-butylfuran-2,5-dione **11** (1.6%). Further, interestingly, the adduct $[Fe(L4)(DBC)]^+$ generated in acetonitrile and DMF solvents reacts (k_{O_2}: DMF, 2.6×10^{-2}; CH_3CN, 2.4×10^{-3} M^{-1} s^{-1}) more slowly than its diazepane analogue $[Fe(L1)(DBC)]^+$ does in the same solvents. The higher Lewis acidity of the iron(III) center in **4** (cf. above) would be expected to form a stronger $Fe-N_{py}$ bond, and hence, the nucleophilic attack of substrate-bound dioxygen on iron(III) center by displacing the strongly bound pyridine nitrogen or carbonyl oxygen of DBC^{2-} is unfavorable (Scheme 5). Also, obviously the attack of O_2 on the iron(III) center in the adduct to yield extradiol cleavage product is not facilitated, thus leading to a lower rate of oxygenation of $[Fe(L4)(DBC)]^+$ to give intradiol cleavage product in lower yield. On the other hand, the dissociation of $Fe-N_{py}$ or Fe−O(DBSQ) bond in the sterically constrained DBC^{2-} adducts of **1**−**3** with cis-β configuration is facile. This major difference in the nature of catechol cleavage products obtained and hence the cleavage pathway (selectivity) may be traced to the difference in the ability of the ligands to confer cis-α or cis-β configuration and hence the availability of octahedral coordination sites for the peroxo coordination. The regiospecificity of oxidative cleavage is thus determined by the binding of catecholate anion, whether it binds in the singly or doubly deprotonated form, and also the ligand steric and electronic effects and hence the nature of the dioxygen species that attacks the bound semiquinone form of DBC^{2-}.

Scheme 5. Proposed Mechanism of Oxygenation of $[Fe(L4)(DBC)]^+$ Using O_2 to Produce Extradiol Cleavage Products

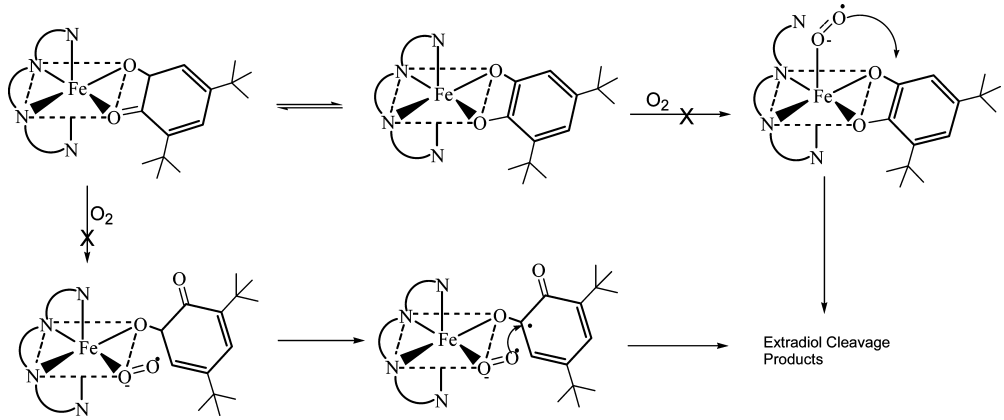

Conclusions and Relevance to Catechol Dioxygenases. The iron(III) complexes of three linear diazapane-based 4N ligands containing two (6-methyl)pyridylmethyl or pyridylmethyl or quinolylmethyl arms have been generated in situ and characterized by ESI-MS, electronic, and EPR spectral and electrochemical techniques. One of the tetrachlorocatecholate (TCC^{2-}) adduct of these complexes exhibit a distorted octahedral iron(III) coordination geometry with a *cis*-β configuration. The iron(III) complexes interact with the substrate 3,5-di-*tert*-butylcatechol (H_2DBC) in the presence of 1 equiv of Et_3N as base to form the adduct $[Fe(L)(HDBC)]^{2+}$ in which monoanionic $HDBC^-$ is coordinated in a bidentate fashion, as revealed by the absorption spectral and pH titration studies. Remarkably, all these adducts afford extradiol cleavage products (2-pyranone) exclusively (34.6−85.5%). On the other hand, the adducts $[Fe(L)(DBC)]^+$ generated by using 2 equiv of Et_3N or 1 or 2 equiv of piperidine show a lower extradiol cleavage selectivity. The exclusive extradiol cleavage products elicited for H_2DBC adducts of the present complexes are in contrast to the major amount of intradiol cleavage products elicited for one of the ethylenediamine analogues with *cis*-α configuration and for other previously reported iron(III) complexes of tetradentate tripodal and linear 4N ligands. Thus, the cleavage products obtained for the present iron(III) complexes depend strongly upon the ligand architecture as well as the mode of coordination of catecholate substrate to iron(III), as determined by the solvent and the base used to deprotonate the substrate.

Acknowledgment. We sincerely thank the Department of Science and Technology, New Delhi, for supporting this research [Scheme No. SR/S1/IC-45/2003] and for the award of Ramanna Fellowship to M.P. and the Council of Scientific and Industrial Research, New Delhi, for a Senior Research Fellowship to R.M. We thank Dr. Balachandran Unni Nair, Central Leather Research Institute, Chennai, for providing ESI-MS facility.

Supporting Information Available: The EPR spectra, electronic spectra of kinetics, electrochemical table (PDF), and crystallographic data in CIF format for **1a**. This material is available free of charge via the Internet at http://pubs.acs.org.

IC702410D